IONOSPHERE DIRECT MEASUREMENTS SATELLITE
S-30

7 August 1960

N-90,000

[redacted]

NATIONAL AERONAUTICS AND SPACE ADMINISTRATION

Washington, D. C.

IONOSPHERE DIRECT MEASUREMENTS SATELLITE

S-30

1. TASK

Ionosphere Direct Measurements Satellite, Payload S-30, Juno II

2. PROJECT

Ionosphere

3. PROGRAM

Geophysics

4. PAYLOAD MANAGER

R. E. Bourdeau, Goddard Space Flight Center

ALTERNATE MANAGER

J. L. Donley, Goddard Space Flight Center

5. PAYLOAD SYSTEMS GROUPS

5.1 Marshall Space Flight Center

5.2 Goddard Space Flight Center

6. PARTICIPANTS

6.1 Marshall Space Flight Center

W. B. Greever	MSFC Project Engineer
H. W. Kampmeir	Antenna
H. M. Pfaff	Mechanical, Despin
P. R. Youngblood	Power Supply, Network wiring

6.2 Goddard Space Flight Center

G. P. Serbu	Ion Trap, Langmuir Probe Experiment
J. L. Donley	Electric Field Meter Experiment
J. A. Kane	RF Impedance Experiment
W. M. Alexander	Micrometeorite Experiment
J. S. Albus	Aspect System
C. B. House	Payload Telemetry
D. S. Hepler	Payload RF
R. C. Waddel	Payload Instrumentation

D. H. Schaeffer	Payload Instrumentation
J. Schaffert	Payload Instrumentation
W. W. Conant	Instrumentation Coordinator
H. E. Evans	Payload Sensors
V. R. Simas	Data Acquisition
C. J. Creveling	Data Reduction
C. R. Hamilton	Coordinator

6.3 NASA Headquarters

I. Cherrick	Satellite and Sounding Rocket Programs
W. E. Williams	Space Flight Operations

6.4 Commercial Contractors

Keithley Corporation	Electrometers
Elgin Micronics	Mechanical Commutator
Aero-Geo-Astrophysics Corporation	Command Receiver
Labko Scientific, Incorporated	Micrometeorite Instrumentation

7. OBJECTIVES

The major objective of the S-30 satellite is the study of the temporal and spatial distribution of ionospheric parameters at altitudes between 320 and 1280 kilometers (200 and 800 nautical miles). The ionization which will be investigated consists of particles with low or thermal energies, a group which exerts the greatest influence on communications.

The S-30 ionosphere experiments differ from those in other NASA-planned ionosphere satellites in that they do not depend upon radio propagation. They are all plasma probes which sample the vehicle environment with data transported over the telemetry link. Plasma probes have two major advantages over propagation methods: they measure considerably more ionospheric parameters, and they are much less sensitive to rapid time variations of ionospheric conditions. On the other hand, the success of the experiments depends upon competent evaluation of the disturbance created in the medium by the presence of the vehicle, a factor which does not affect propagation methods appreciably.

The ionospheric parameters which will be studied include the concentrations of electrons and positive ions, the electron temperature, and the mass distribution of the positive ions. Simultaneous measurement of electron and ion concentration will resolve the question of the neutrality of the medium. Electron temperature data, when compared with kinetic gas temperatures obtained by other observers, will resolve the important question of thermodynamic equilibrium. If equilibrium is

established, the measurement of electron temperature could be the most convenient method of studying temperature distributions in the outer regions of space. Studies of the ion mass distribution will establish the altitude of the base of the exosphere, and will be important to theories of magnetohydrodynamics.

A secondary objective is the measurement of the charge accumulation on the satellite surfaces. These data can be related to electrical drag. Consequently, they are important to studies of the density of the medium, which presently are being computed from satellite orbital decay observations neglecting electrical drag. This is particularly important because of the possibility of high satellite potentials in the Van Allen Radiation Belt.

Other secondary objectives of the satellite are the measurements of the frequency, momenta and energies of micrometeorite impact. The momentum range which will be scanned will be considerably larger than that of previous satellites. The energy measurement experiment will be an improved version of one used earlier in a rocket flight. Comparison of the energy and momentum data will permit separate determination of the masses and the velocities of the micrometeorite particles. Since satellite aspect will be measured, the velocity vectors of the particles also will be ascertained. Because of the low perigee, observations will be made of the effects of "sputtering" on the surface of the micrometeorite energy detector. "Sputtering" is defined as erosion of the vehicle surfaces by impingement of all types of particles including the micrometeorites themselves.

8. DESCRIPTION OF EXPERIMENTS

The following is a list of the S-30 scientific experiments and their individual objectives:

Experiment	Measured Parameters
RF Impedance Probe	Electron Concentration
Two Single-Grid Ion Traps	Positive Ion Concentration
Two Multiple-Grid Ion Traps	and Mass Distribution
Two Langmuir Probes	Electron Temperature
Electric Field Meter	Satellite Charge Distribution
Two Microphones	Frequency and Momenta of Micrometeorite Impacts
Photomultiplier	Frequency and Energies of Micrometeorite Impacts

The positioning of the sensors on the satellite is illustrated in Figures 1 and 2. Also shown are the locations of aspect sensor used for supporting information.

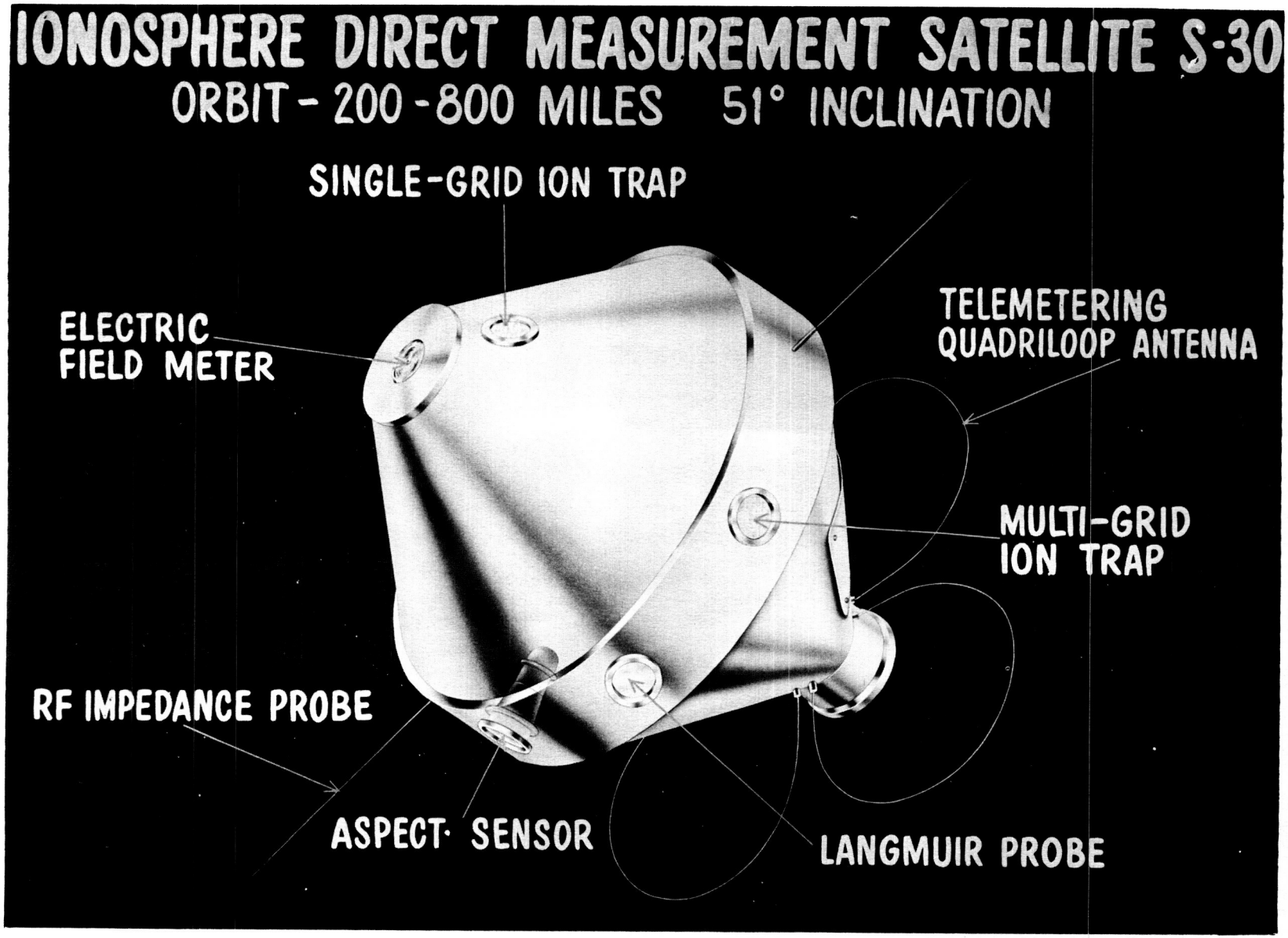

Figure 1 - Sensor locations

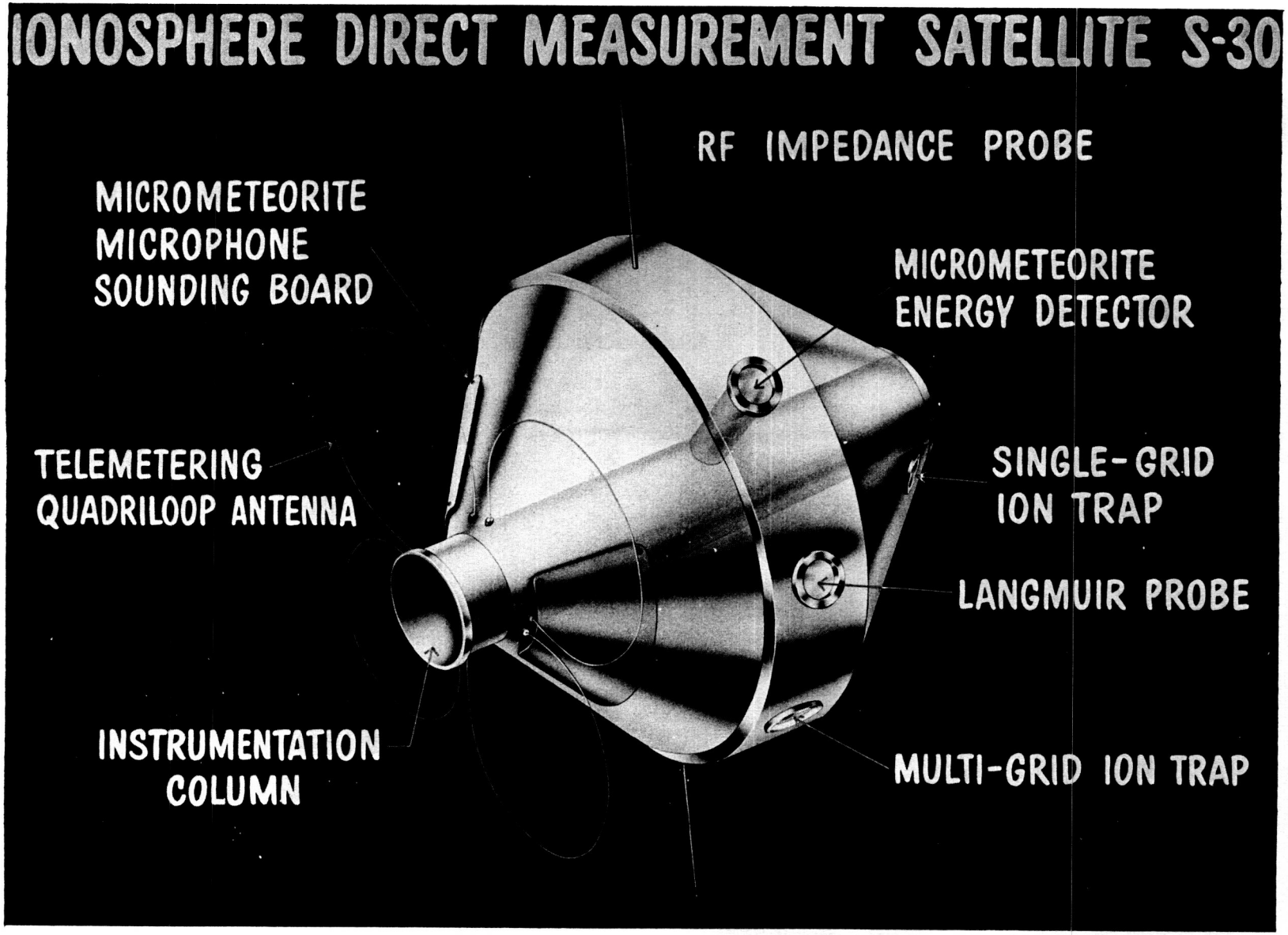

Figure 2 - Sensor locations

8.1 The Radio-Frequency Impedance Probe Experiment

The objective of this experiment is the measurement of electron concentration. This is accomplished by comparing the in-flight capacitance (C) of the sensor with its free-space value (C_o). The latter capacitance is obtained from preflight measurements on a simulated satellite configuration. The sensor, located on the satellite's equator, is a shortened dipole antenna, each half of which is 10 feet long.

The electron concentration (N_e) is computed from the simplified Appleton-Hartree formula which relates N_e to the dielectric constant (K) of the medium. Specifically, since the effects of the earth's magnetic field are neglected, the formula used is

$$K = \frac{C}{C_o} = 1 - \frac{81\, N_e}{f^2}, \qquad (1)$$

where f is the frequency (6.5 Mc) of the voltage applied to the antenna probe. It should be emphasized that the amount of power radiated is negligibly small. Since C_o is measured before flight and f is known, it is necessary only to measure C to obtain electron concentration.

A measurement of C is made every 40 milliseconds, so that the experiment can actually search out ionospheric heterogeneities with dimensions of the order of 300 meters. This capability is important to theories of the ionosphere, particularly to the understanding of solar disturbances which disrupt communications.

The experiment has been tested in vertical sounding rockets where, as expected, some error in the absolute measurement of N_e was observed owing to an ion sheath which forms about the sensor. Although the rocket results can be used to analytically correct for this error, this will be checked in S-30 by occasionally placing a variable bias with a 0.2 second period on the antenna to collapse the ion sheath. The variable bias will be applied on command.

8.2 The Single-Grid Ion Trap Experiment

The objectives of this experiment are the measurements of positive ion concentrations and mass distributions. The techniques involved are very similar to vacuum tube techniques. The ionosphere provides a near vacuum and also acts as the filament or ionization source. It is only necessary then to provide the grid and the plate or collector to complete the construction of a vacuum tube in space, and consequently to study the ionization in the immediate vicinity of the satellite.

The two single-grid ion-trap sensors are located near the forward end of the spin axis (Figure 1). Two are used because the experiment is attitude sensitive and simultaneous comparison of the data from each sensor assists in ascertaining the attitude. Each sensor is in the form of a cylinder 3 inches in diameter. Each

consists of a grid flush with and insulated from the satellite skin behind which is located a circular collector. The grids have approximately 90 percent transparency.

Figures 3a and 3c illustrate the basic principle of the experiment. The collector is biased negatively to eliminate electron current. A sweep voltage (V_g) varying between -5 and +25 volts is applied between the grid and satellite skin. The desired information is the collector current (I_c) as a function of the grid voltage. The ion concentration (N_+) is computed from the measured collector current at low values of V_g according to:

$$I_c = I_{max} = N_+ \, ev \, A \, , \tag{2}$$

where e (a constant) is the electron charge, v the satellite velocity and A the effective collector area. Equation 2 is valid only if the ion trap is pointed along the satellite velocity vector. For this reason, the satellite aspect is measured and two ion traps are included.

Because the satellite velocity is large compared with the average ion velocity, the ions will have a kinetic energy (relative to the satellite) proportional to their mass. For this reason, it is possible to discern the mass distribution from the shape of the ion trap volt-ampere curve. The potential (V_r) required to retard or stop an ion with a mass of m_+ is given by:

$$V_r = \frac{m_+ v^2}{2} . \tag{3}$$

Figure 3c illustrates a typical volt-ampere curve for a medium containing a single ionic constituent. The satellite potential relative to the medium (V_s) will be measured by the Langmuir probe as described below. The retarding potential (V_r) is obtained by subtracting V_s from the measured grid voltage at the point on the volt-ampere curve where the collector current is $I_{max}/2$. The mass of the ion can then be computed from Equation 3. If several types of ions are present, they will be detected because the volt-ampere curve will have a corresponding number of plateaus.

Data from both single-grid ion traps are telemetered simultaneously. Twenty-four points are telemetered for each volt-ampere curve. This is accomplished every 0.2 seconds (the period of V_g) so as to obtain a complete curve for a minimum change in satellite position. Since it is important also to obtain a complete curve for a negligible change in satellite attitude, the satellite spin rate will be reduced to an orbital value of less than 30 rpm.

8.3 The Multiple-Grid Ion Trap Experiment

The objectives and the basic principles of this experiment are the same as those of the single-grid ion trap experiment described above. The experiment is illustrated in schematic form in Figure 3b. The accompanying instrumentation is

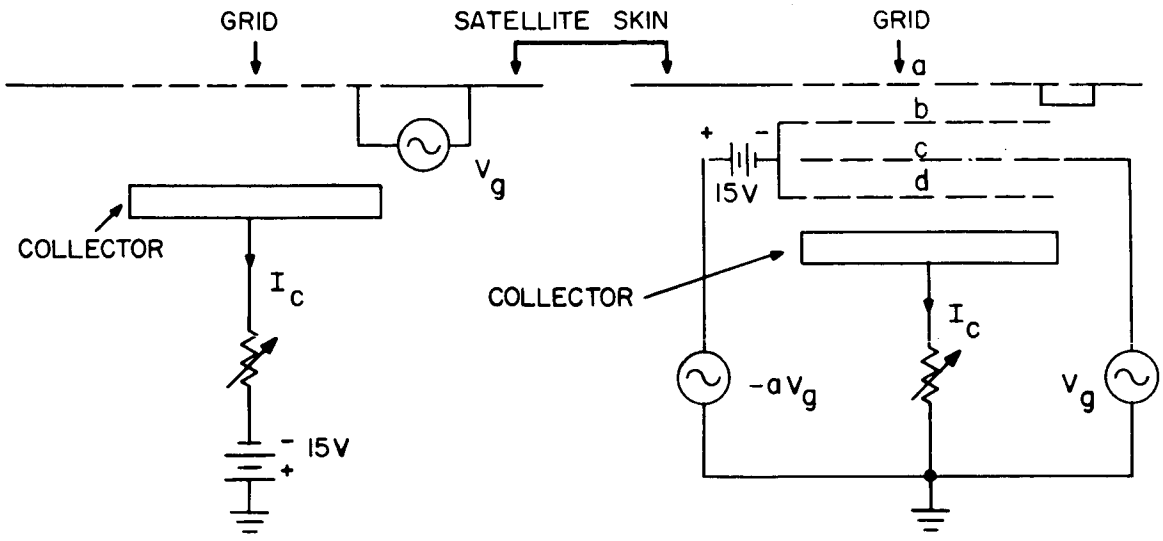

(a) SINGLE–GRID ION TRAP

(b) MULTI–GRID ION TRAP

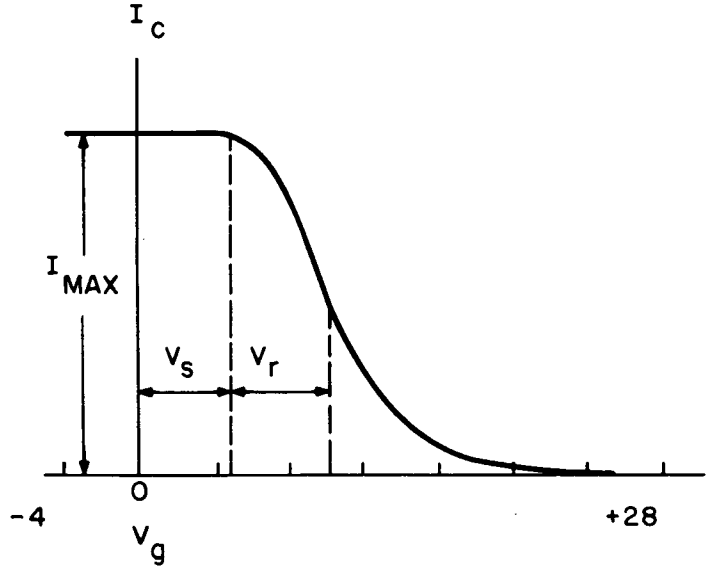

(c) TYPICAL VOLT–AMPERE CURVE

Figure 3 - Schematic of ion trap experiments

common and time-shared. Both experiments were calibrated against a cw propagation experiment in vertical sounding rockets.

The two multiple-grid ion-trap sensors are located diametrically opposite from each other on the equator of the satellite (Figure 1). Each sensor consists of four concentric grids and a collector. The outermost grid (a) is connected to the satellite skin. The sweep voltage (V_g) is applied to the third grid (c). The second grid (b) is biased negatively to remove incoming electron current. The fourth grid (d) is biased negatively to remove secondary emission effects from the collector. The most serious form of secondary emission is an outgoing electron current from the collector when it is exposed directly to the sun. A sweep voltage attenuated and 180 degrees out of phase with V_g is applied to grids b and d to eliminate displacement currents. This is not a problem with the single-grid trap because of the larger spacing of the electrodes.

The single-grid ion trap will be sensitive to photoemission while the multiple-grid ion trap will not. Comparison of the data from the two experiments will determine the magnitude of the photoemission current. This is important to the design of any plasma probe planned for interplanetary missions. Measurements of the photoemission current are necessary to predicting the polarity and magnitude of the potential on an interplanetary space vehicle.

8.4 The Langmuir Probe Experiment

The objective of this experiment is the measurement of electron temperature. The basic principles of the experiment are illustrated by Figure 4. Two sensors located diametrically opposite from each other are used. Each sensor consists of a collector in the form of a circular plate flush with and insulated from the satellite skin. The same sweep voltage applied to the ion traps is applied to the collector. In the case of the Langmuir probe both electron and positive ion currents are measured. The collector is surrounded by an annular ring electrically connected directly to the sweep voltage. This ring serves as a guard to reduce leakage.

Figure 4b illustrates a typical volt-ampere curve. For negative values of V_g, the collector current is entirely due to positive ions (I_+). At large positive values of V_g, the collector current is entirely due to electrons (I_{e_o}) and will be equal to the ambient electron current flowing in the ionosphere. In between these two regimes, the collector current includes contributions from both positive ions and electrons. After correction is made for the positive ion current, a logarithmic plot of the curve in this region yields the electron temperature. The point at which the electron current saturates is the point where the collector is at plasma potential and thus is a measure of the satellite potential (V_s).

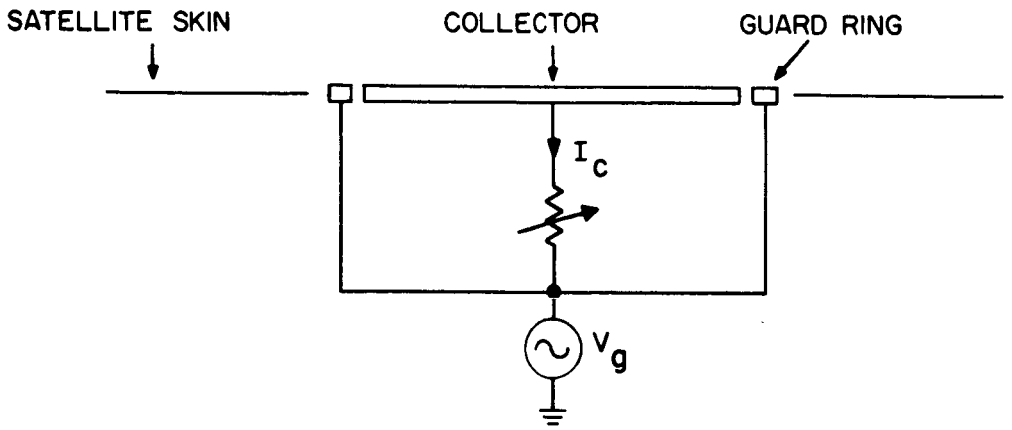

(a) LANGMUIR PROBE

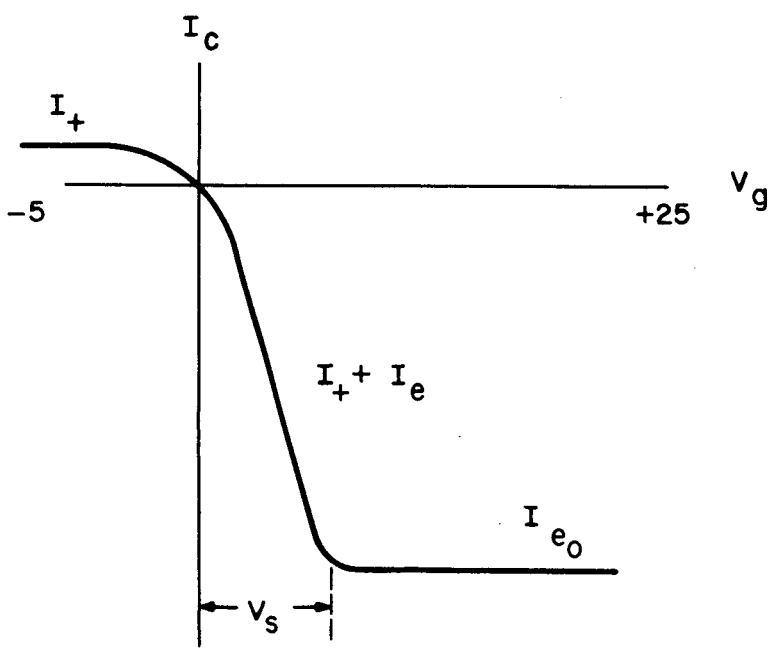

(b) TYPICAL VOLT-AMPERE CURVE

Figure 4 - Schematic of Langmuir probe experiment

8.5 The Electric Field Meter Experiment

The objective of this experiment is the measurement of the distribution of charge which accumulates on the satellite surface. The sensor, located directly on the spin axis, is termed a rotating-shutter type electric field meter. It consists of two basic elements: an exposed four-bladed motor-driven shutter (rotor) grounded to the satellite skin by the use of brushes, and a four-bladed stator or sensor (located behind and having the same configuration as the rotor) which is returned to ground through a resistive load R. The rotor speed is accurately controlled at 9000 rpm. A prototype of the sensor is shown in Figure 5. It is similar to one flown recently in a vertical sounding rocket except that the driving motor is equipped with lubrication-free bearings and high-altitude brushes to insure long-term operation in a vacuum.

The electric field meter is designed to measure the electric field due to the ion sheath which forms around the satellite. This electric field is proportional to the ratio of the potential of the satellite relative to the medium (V_s) and the thickness of the sheath. Since the medium is ionized, a second stator signal will be produced by current which flows between the medium and the satellite. This current would be zero at every point on the satellite surface in the absence of such effects as photoemission. However, since such effects are present a net current with density (J) can be expected at specific points. The signals due to the electric field (V_E) and to the diffusion current (V_J) will be in quadrature and thus can be separated by phase discrimination. Their amplitudes are given by

$$V_E = \epsilon\, E\, AwR, \tag{4}$$

and

$$V_J = JAR, \tag{5}$$

where ϵ is a constant, A is the area of the stator, and w is the angular rotor frequency. The measured electric field can then be related to the vehicle charge distribution. It can be seen from Equations 4 and 5 that the effects of the diffusion current on the measurement of E can be reduced by a high rotor speed. A synchronous wave is developed at the back end of the motor shaft. This wave is used as a reference for separation of V_E from V_J and to detect the polarity of E and J. A block diagram of the experiment is shown in Figure 6.

The S-30 electric field meter system will measure electric fields up to 10,000 volts per meter. It has a noise equivalent of less than 5 volts per meter. As with all field meters of this type it has a residual field or residue produced by rotor-to-stator contact potential. The residue drift is less than 5 volts per meter even though a close rotor-stator spacing (3 mm) is maintained.

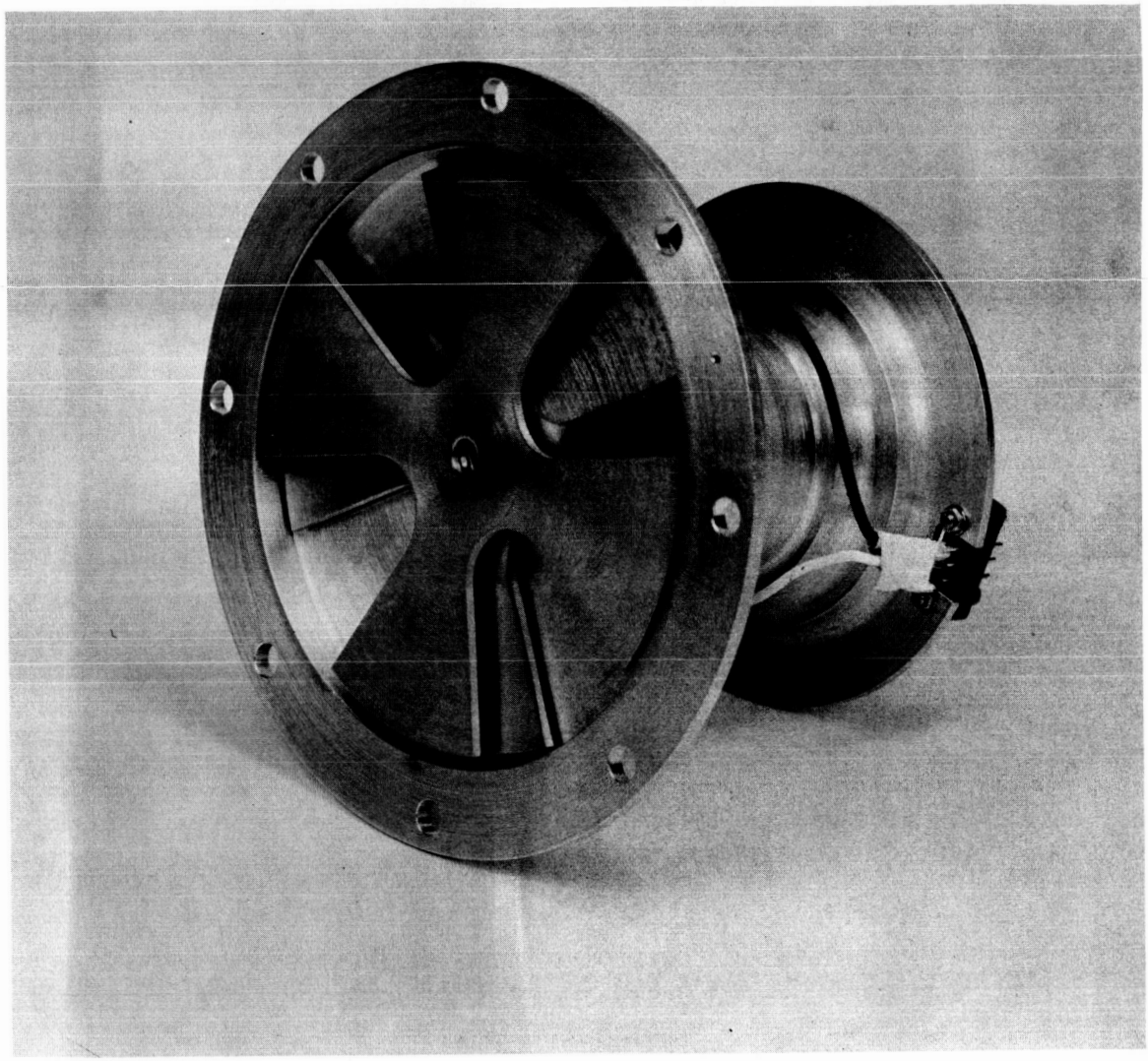

Figure 5 - Prototype electric field meter for S-30

8.6 Micrometeorite Photomultiplier Experiment

The objects of this experiment are twofold: (1) To measure the light energy emitted as a micrometeorite impinges upon a surface and to relate this measured energy to the ambient kinetic energy of the particle and (2) to determine the erosive effects of micrometeorite impact.

The sensor (Figure 7) is a conventional "end-type" ruggedized 6199 photomultiplier with a 1000A evaporated layer of aluminum on the front surface. A micrometeorite particle penetrates the aluminum coating and registers its visible-light energy on the photocathode. The resultant pulse will vary in length and amplitude as a function of the micrometeorite's kinetic energy. The pulse is amplified, integrated, and presented to the telemetry encoder as an output pulse whose amplitude is in proportion to the amplitude and total energy, respectively of the original pulse. The system has a dynamic range of three decades.

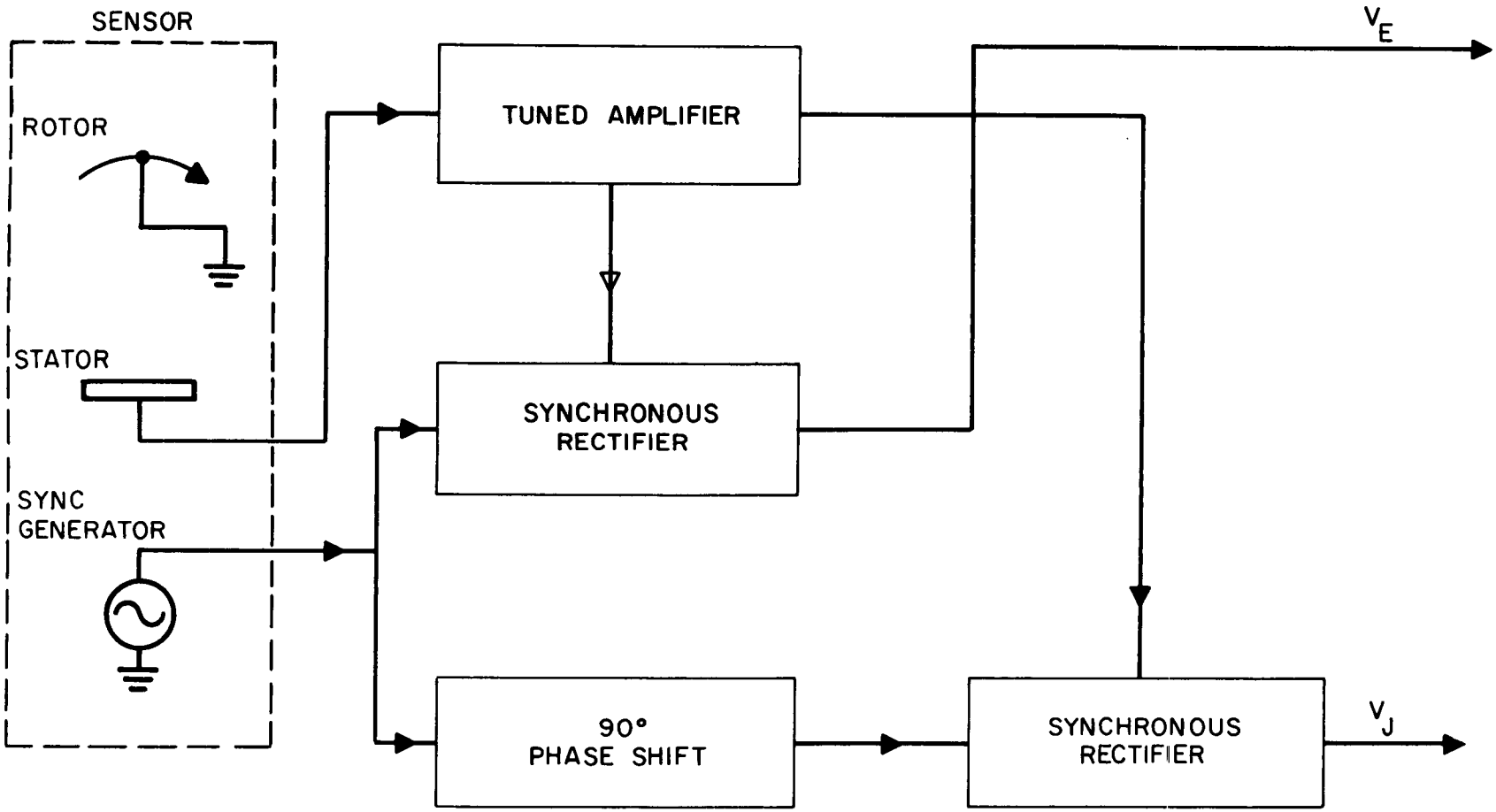

Figure 6 - Block diagram of electric field meter experiments

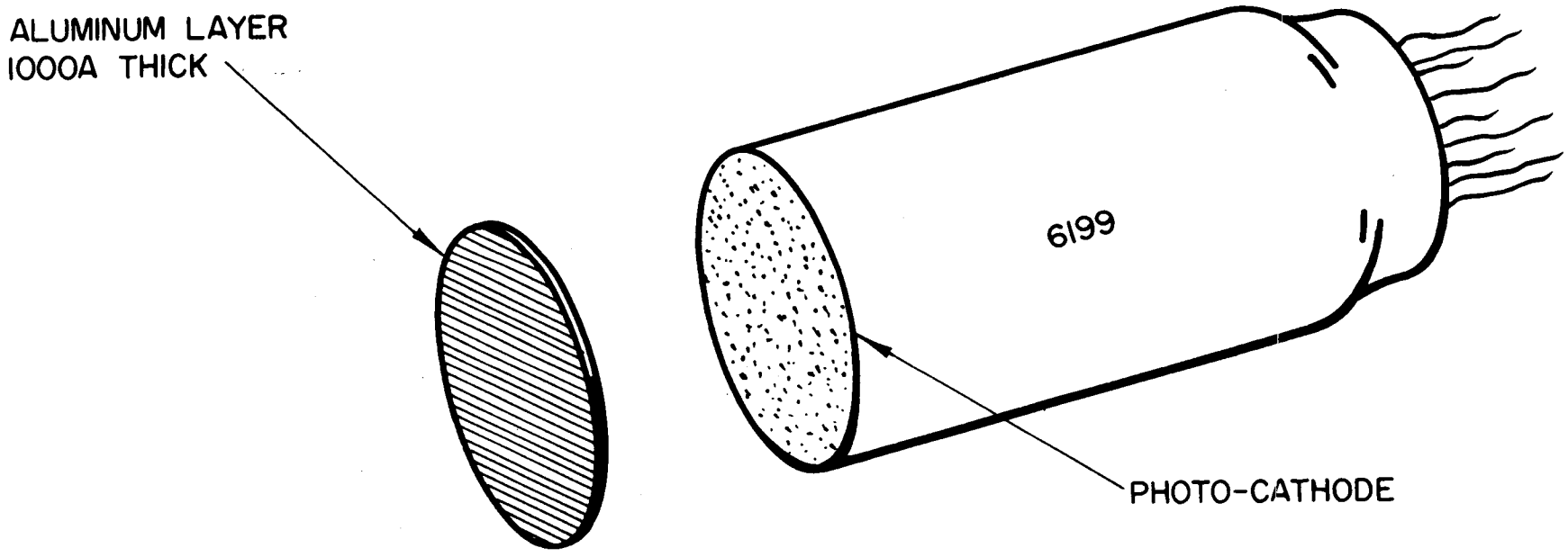

Figure 7 - Micrometeorite photomultiplier

The maximum sensitivity of the sensor to light pulses is of the order of 10^{-3} erg. If the assumption is made that the micrometeorite impinging on the surface transforms its energy in a similar ratio of heat, light, and ionization to that of a meteorite traversing an atmosphere, the sensor's maximum sensitivity can be put in terms of detection of impacts of particles of $<10^{-15}$ grams having a velocity of only 20 km/sec.

For each measurable micrometeorite impact a portion of the aluminized coating will be removed. Gradually, the photomultiplier will begin to register the amount of light energy transmitted through the layer from extraneous light sources such as direct sunlight, reflections from the moon, the earth and the night sky. Since the intensity and characteristics of these sources are known and since the number and energy of micrometeorite impacts will have been recorded, one can obtain a measurement of the erosive effects of a single micrometeorite.

8.7 The Micrometeorite Microphone Experiment

The objective of this experiment is the measurement of the frequency and momentum of micrometeorite impact. The micrometeorite targets are two "sounding boards" located on the lower cone of the satellite (Figure 2), acoustically insulated from the satellite skin. Attached to each sounding board is a microphone which senses the impulse occurring when a micrometeorite collides with the sounding board. By preflight calibration the detected impulse can be related to the momentum of the incoming particle. The maximum detectable sensitivity is 10^{-4} dyne-second and the system has a dynamic range of three decades.

8.8 Overall Payload

The configuration of Satellite S-30 is very similar to that of Explorer VII. As illustrated in Figures 1 and 2, it is in the form of two truncated cones with their bases attached to a cylindrical equator. The satellite is 30 inches in height and diameter and the overall weight in orbit will be approximately 90 pounds. The outer shell is constructed of aluminum. The orbit injection sequence as illustrated by Figure 8 is as follows: separation of satellite from fourth stage rocket, first-stage despin, disposal of despin mechanism, release of rf impedance probes which simultaneously acts as second stage despin. The payload consists of:

8.8.1 Timer and Separation Mechanism

A battery-operated timer is attached to the base of the instrument column. The timer performs two functions: it actuates a release mechanism separating the payload from the fourth stage rocket approximately two minutes after fourth stage burnout and it initiates first-stage despin shortly thereafter.

8.8.2 First-Stage Despin Mechanism

The function of this mechanism is to reduce the payload spin rate from 450 to 100 rpm. The mechanism consists of two weighted wires wrapped around

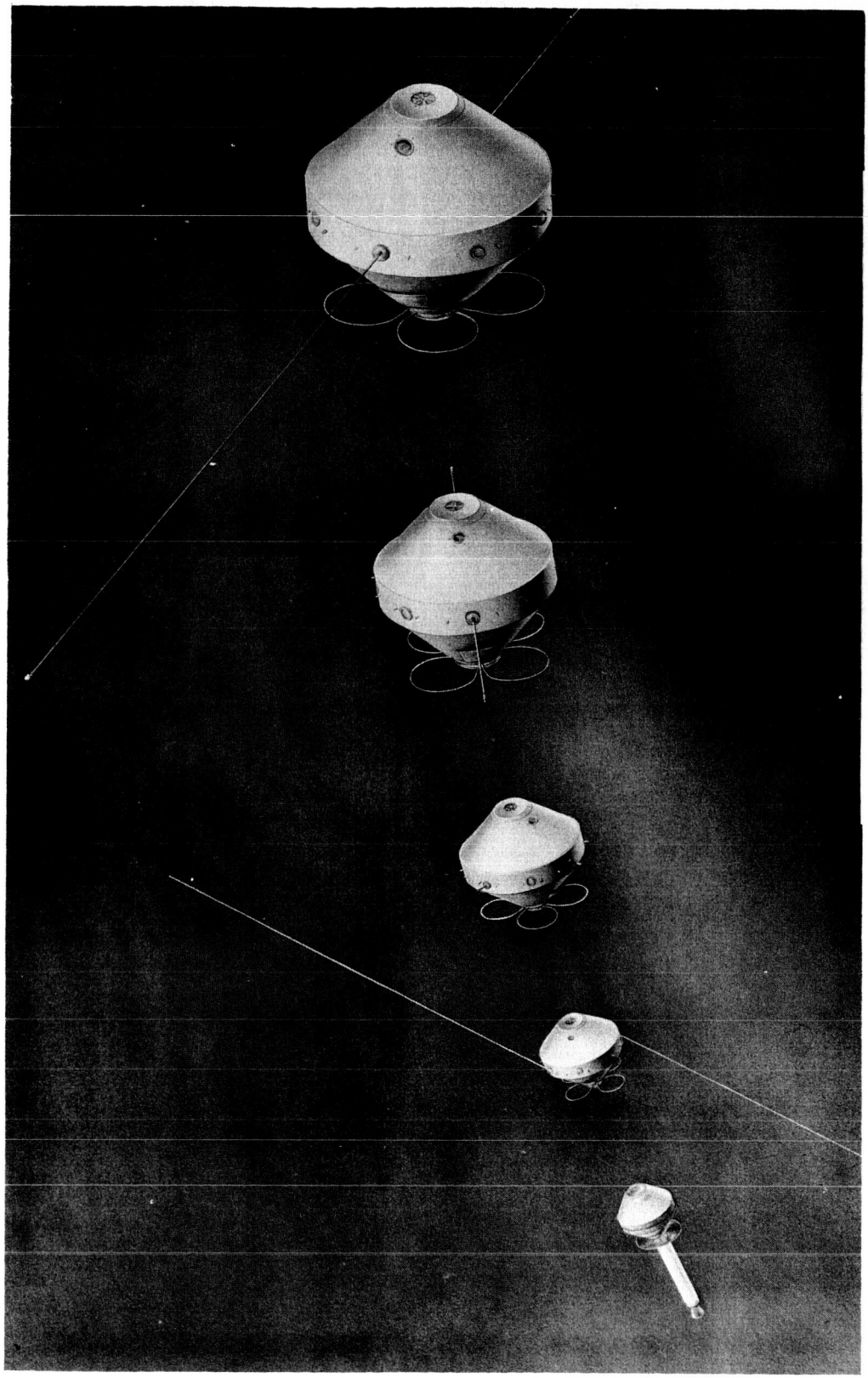

Figure 8 - Orbital injection sequence, satellite S-30

the equator. A squib causes the wires to unwind. At the completion of this first-stage despin operation, the wires are released automatically from the payload. The release operation in turn starts the extension of the rf impedance probe which simultaneously acts as second-stage despin.

8.8.3 Batteries

Eight boxes (Figure 9) containing mercury batteries are located on the periphery of the satellite's equator.

8.8.4 Thermal Coatings

8.8.5 Balance Weights

8.8.6 Sensors

8.8.6.1 RF impedance probe:

As shown in Figure 1, the rf impedance probe consists of two 10-foot whips located diametrically opposite each other on the satellite's equator. The two whips are weight-loaded at the ends and are extended by centrifugal force. A specially designed mechanical system (Figure 10) acts as a governor which fully extends the wires at a constant rate in 10 seconds. The process of extending the whips reduces the payload spin rate from 100 rpm to a target design value of 30 rpm. Simulated magnetic field tests conducted by Marshall Space Flight Center (MSFC) indicate that this rate will reduce to less than 10 rpm at the end of the satellite's active life.

8.8.6.2 Two single-grid ion traps:

The two traps are located near the spin axis (Figure 1). Each trap (Figure 11) is a cylinder 3 inches in diameter and 1 inch deep with a 3-1/2-inch mounting flange. The exposed grid is a 1-mil tungsten mesh with 90 percent transparency. A nichrome collector with an effective diameter of 1-5/8 inches is located 1/2 inch behind the grid.

8.8.6.3 Two multiple-grid ion traps:

These two traps (Figure 11) are located diametrically opposite each other on the satellite equator (Figure 1), 45 degrees away from the rf impedance probes. The outer dimensions are the same as the single-grid ion traps. Each trap consists of four grids and a collector concentrically arranged. The spacing between electrodes is 1/8 inch.

8.8.6.4 Two Langmuir probes:

The two sensors are located diametrically opposite each other on the satellite equator, 90 degrees away from the rf impedance probe.

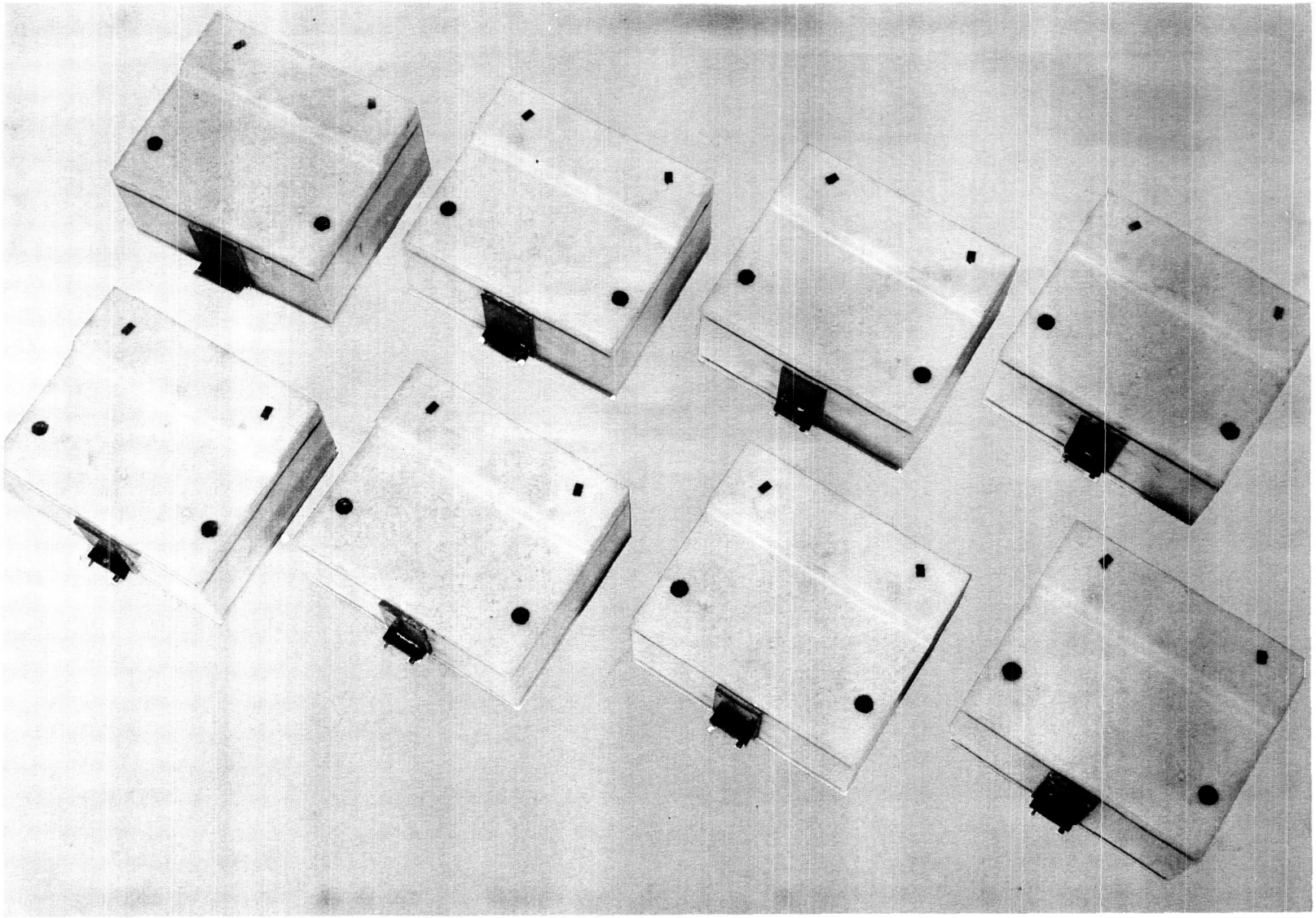

Figure 9 - Battery packs for satellite S-30

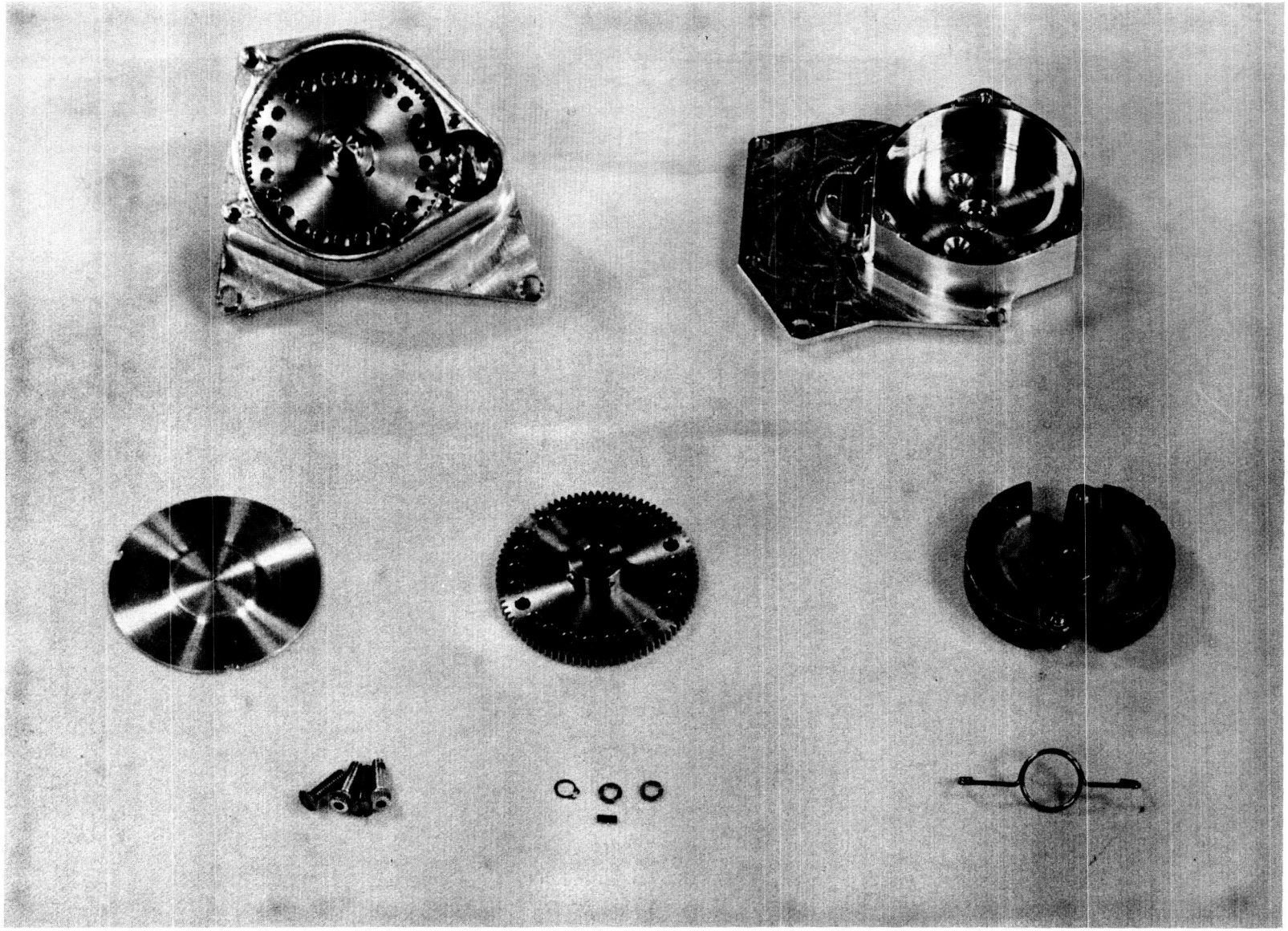

Figure 10 - RF impedance probe release governor

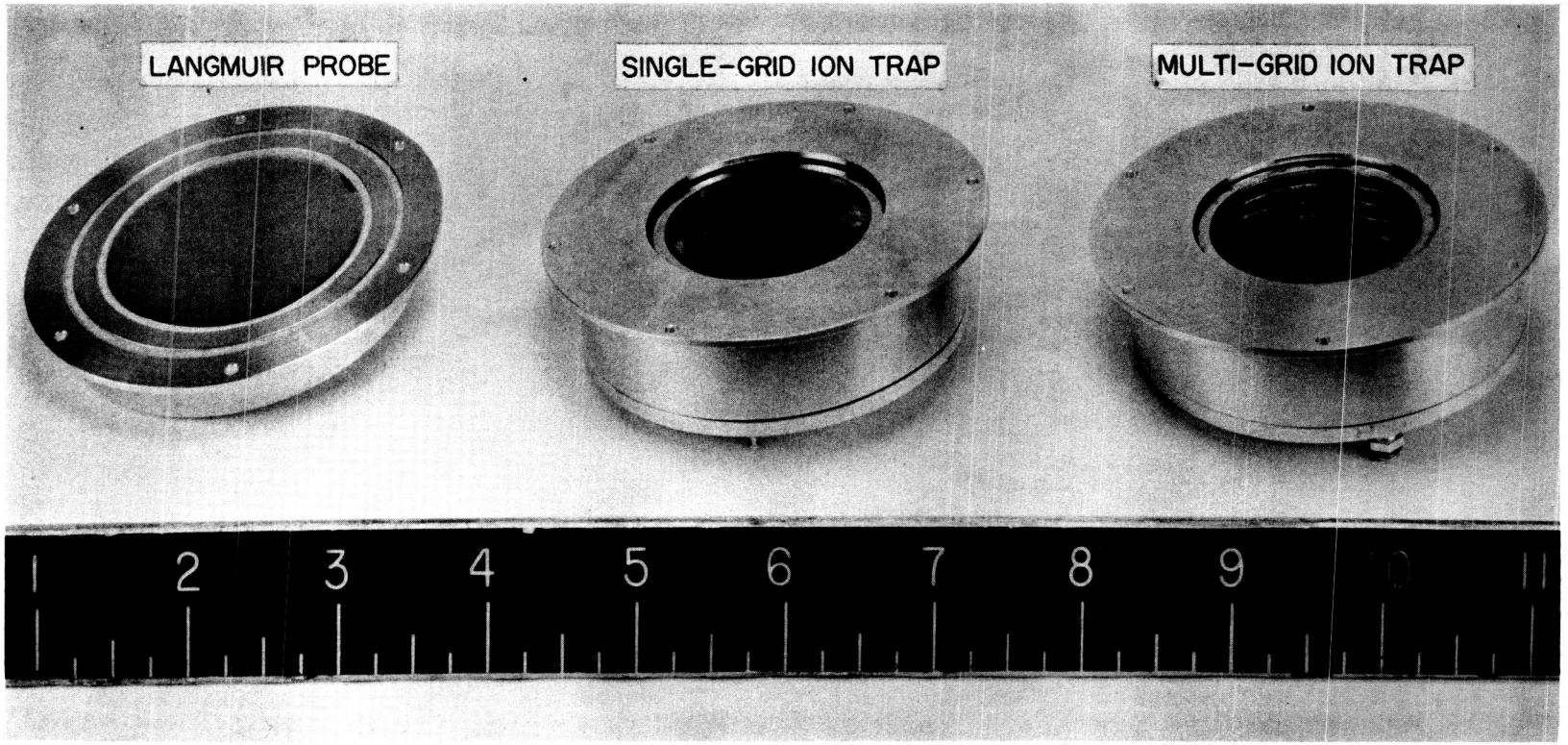

Figure 11 - Ion trap and Langmuir probe sensors

Each sensor (Figure 11) consists of an exposed annular guard ring insulated from the satellite skin. The annular ring surrounds a 2-inch circular collector plate of chromium-plated aluminum. The sensors have a 3-1/4-inch mounting flange and are 5/8 inch deep. Figure 11 is a photograph of one each of the ion trap and Langmuir probe sensors.

8.8.6.5 Electric field meter:

This sensor (Figure 5) is attached mechanically to the instrument column at the forward end of the spin axis. The rotor and stator are 3 inches in diameter, the mounting flange is 4 inches, and the depth of the instrument is 3-1/2 inches. The driving motor is a modified dc permanent-magnet 1/200 hp motor. To obtain reliable operation in a vacuum at the expected pressure and temperature, dry bearings and special high-altitude carbon brushes with molybdenum disulfide rods are used. The unit has been environmentally tested at pressures down to 10^{-6} mm and over a temperature range from -20 to +90°C. With the modifications, it has a life expectancy of at least 25 hours of actual operating time.

8.8.6.6 Micrometeorite photomultiplier:

The location of this sensor is shown in Figure 2. The photomultiplier has an exposed area of approximately 2 square inches and is recessed in a collimating tube 2 inches in diameter. A high-voltage power supply, a pulse amplifier and an in-flight calibration system are attached to the back of the photomultiplier housing (Figure 12).

8.8.6.7 Two micrometeorite sounding boards:

These two trapezpoidal-shaped aluminum sensors are located on the lower satellite nose cone (Figure 1) and have a total area of about 0.1 meter. The sensors are acoustically insulated by use of Teflon. Cemented to each board is a piezoelectric transducer (microphone).

8.8.6.8 Four thermistors:

Four thermistors will be used to monitor temperatures at the following payload locations: battery case, within the instrument column, in the vicinity of the micrometeorite photomultiplier tube, and on the inside of the skin at the equator.

8.8.6.9 Aspect sensor:

This sensor (Figure 13) is located on the satellite equator diametrically opposite from the micrometeorite photomultiplier. It consists of a solar and a horizon tracking unit in the same housing. The solar tracking portion of the sensor consists of two silts behind each of which is

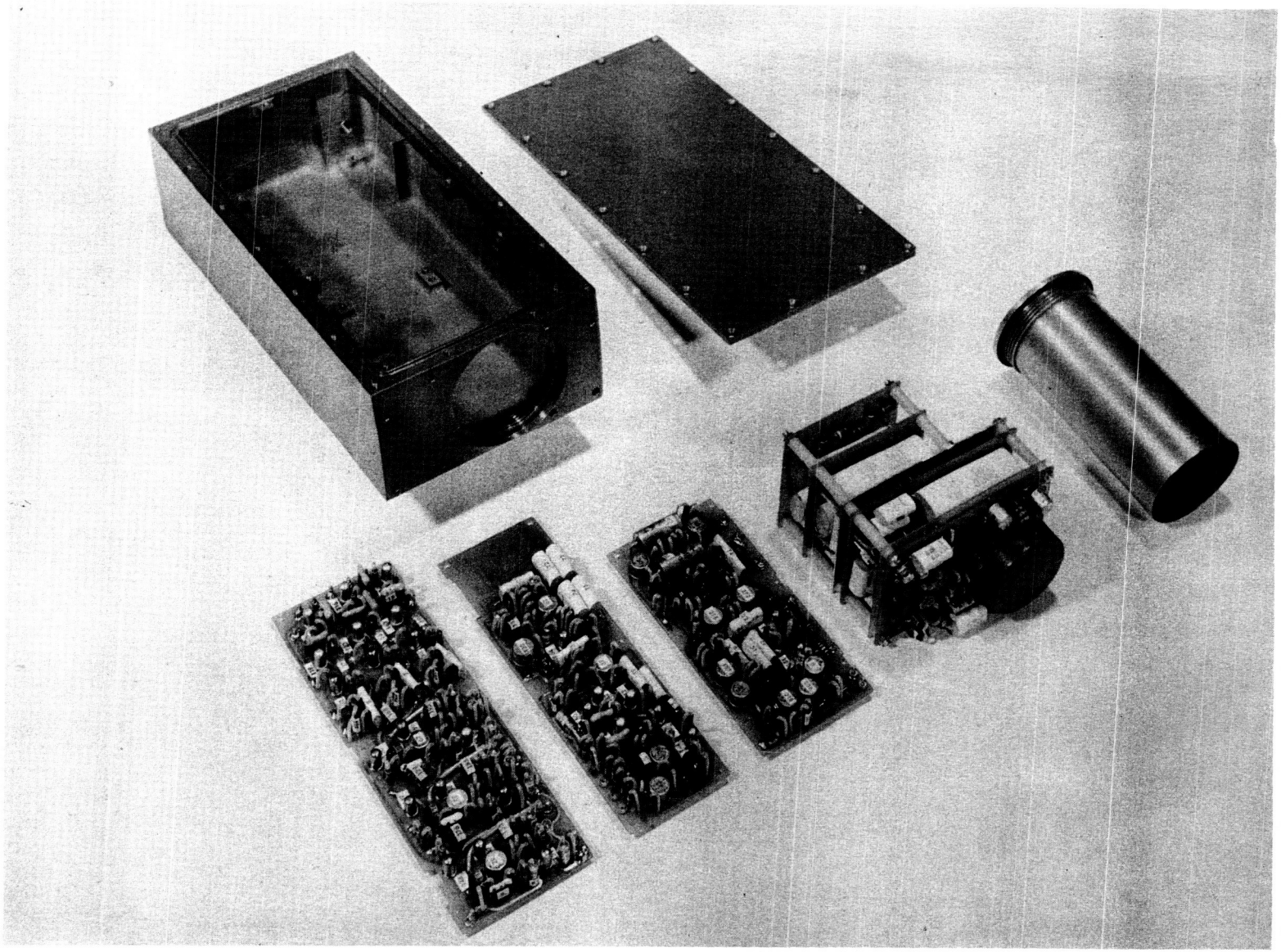

Figure 12 - S-30 photomultiplier micrometeorite detection system

located a photo-sensitive silicon diode (1N217S). One slit is parallel to the spin axis, and the other is slanted approximately 25 degrees. By measuring the time separation of light indication on the two diodes, azimuth and elevation information from the sun are obtained. The horizon seeker consists of two 1N17S diodes behind small apertures appropriately located. The solar and horizon aspect system together are designed to define the satellite orientation to an accuracy of one degree.

8.8.7 Instrument Column

The instrument column (Figure 14) is 19-1/2 inches high and approximately 6 inches in diameter. It consists of 20 modules (Table 1) not counting the separation timer. A brief description of the modules follows:

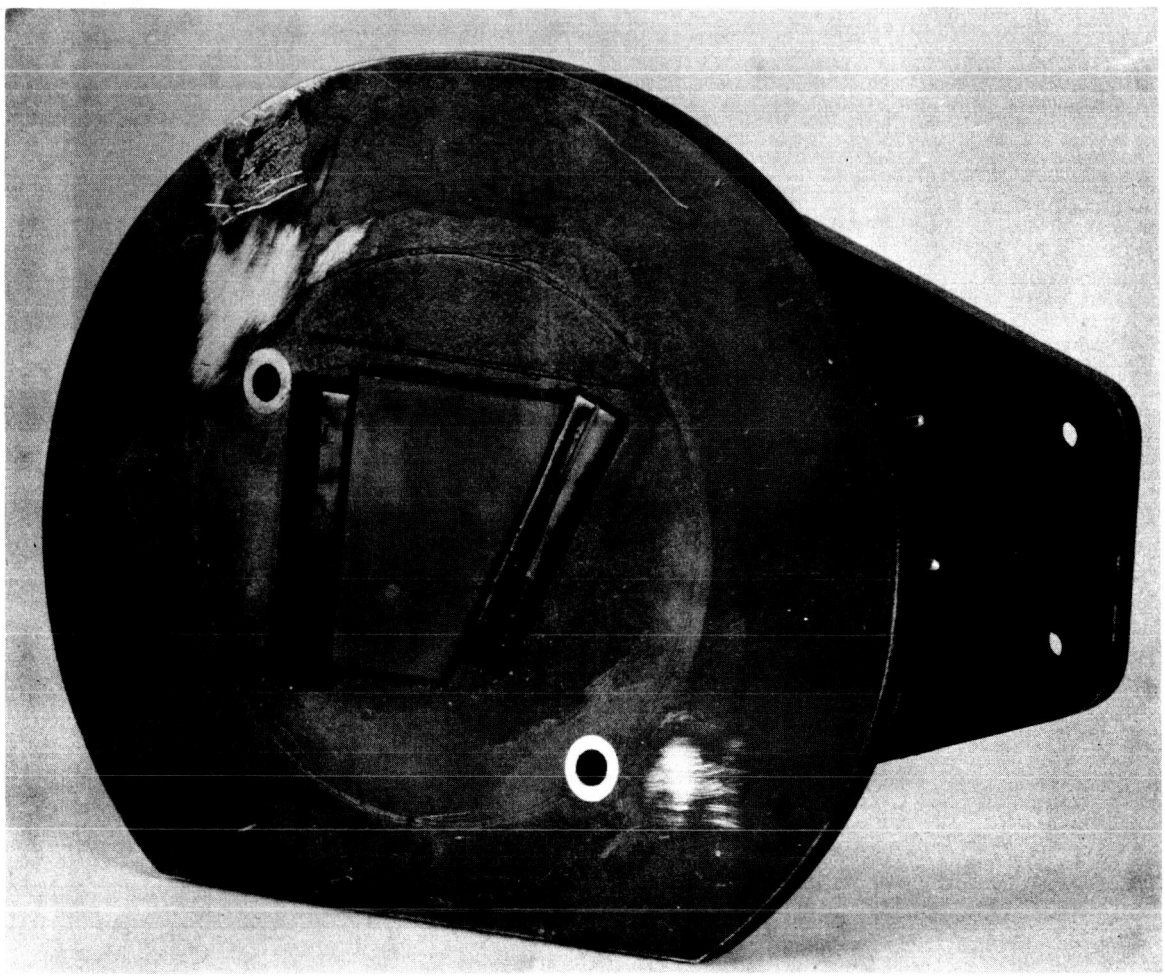

Figure 13 - Aspect sensor

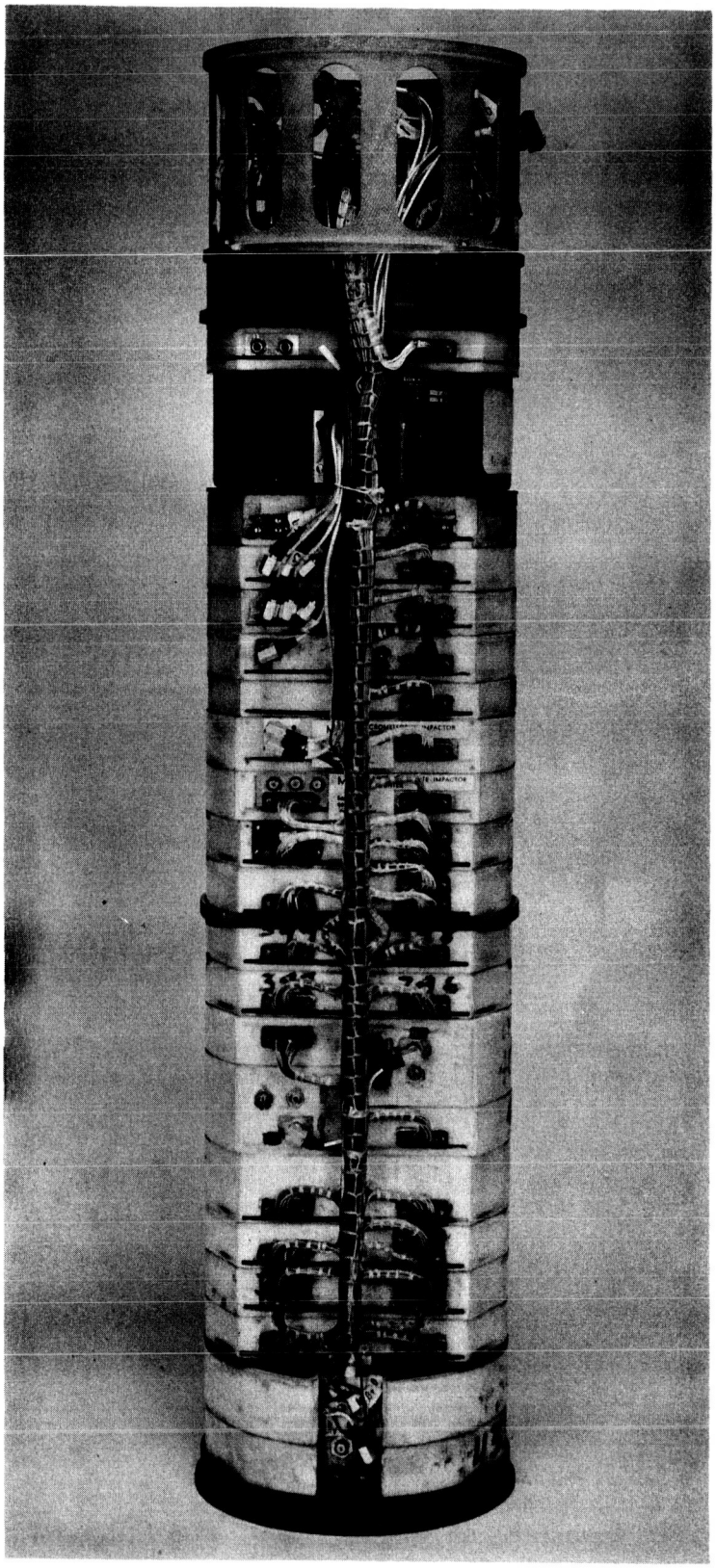

Figure 14 - Instrument column

Table 1

Instrument Column Layout

COMMUTATOR
SWEEP GENERATOR
ELECTROMETER #1
ELECTROMETER #2
FIELD METER AMPLIFIER
COMMAND PROGRAM
METEORITE AMPLIFIER
METEORITE COUNTER
ASPECT-DIGITALIZER
COMPUTER PULSER
ASPECT-RF MEMORY A
ASPECT-RF MEMORY B
RF IMPEDANCE A
RF IMPEDANCE B
OSCILLATOR B
OSCILLATOR A
ENCODER #1
ENCODER #2
COMMAND RECEIVER
TRANSMITTER

8.8.7.1 Sweep generator:

This unit (Figure 15) has two outputs. The first and main output is a repetitive wave varying between -5 and +25 volts every 0.2 seconds. The output impedance is 10,000 ohms. This wave is basic to the ion trap and Langmuir probe experiments. As illustrated schematically in Figures 3 and 4, this output is applied continuously to the grids of the single-grid ion trap sensors, to the third grids of both multiple-grid ion trap sensors to two Langmuir probe collectors. Since the collector currents are required as a function of this sweep voltage, the latter is telemetered on a time-sharing basis with the two electric field meter amplifier outputs by a mechanical commutator inserted prior to telemetry encoding.

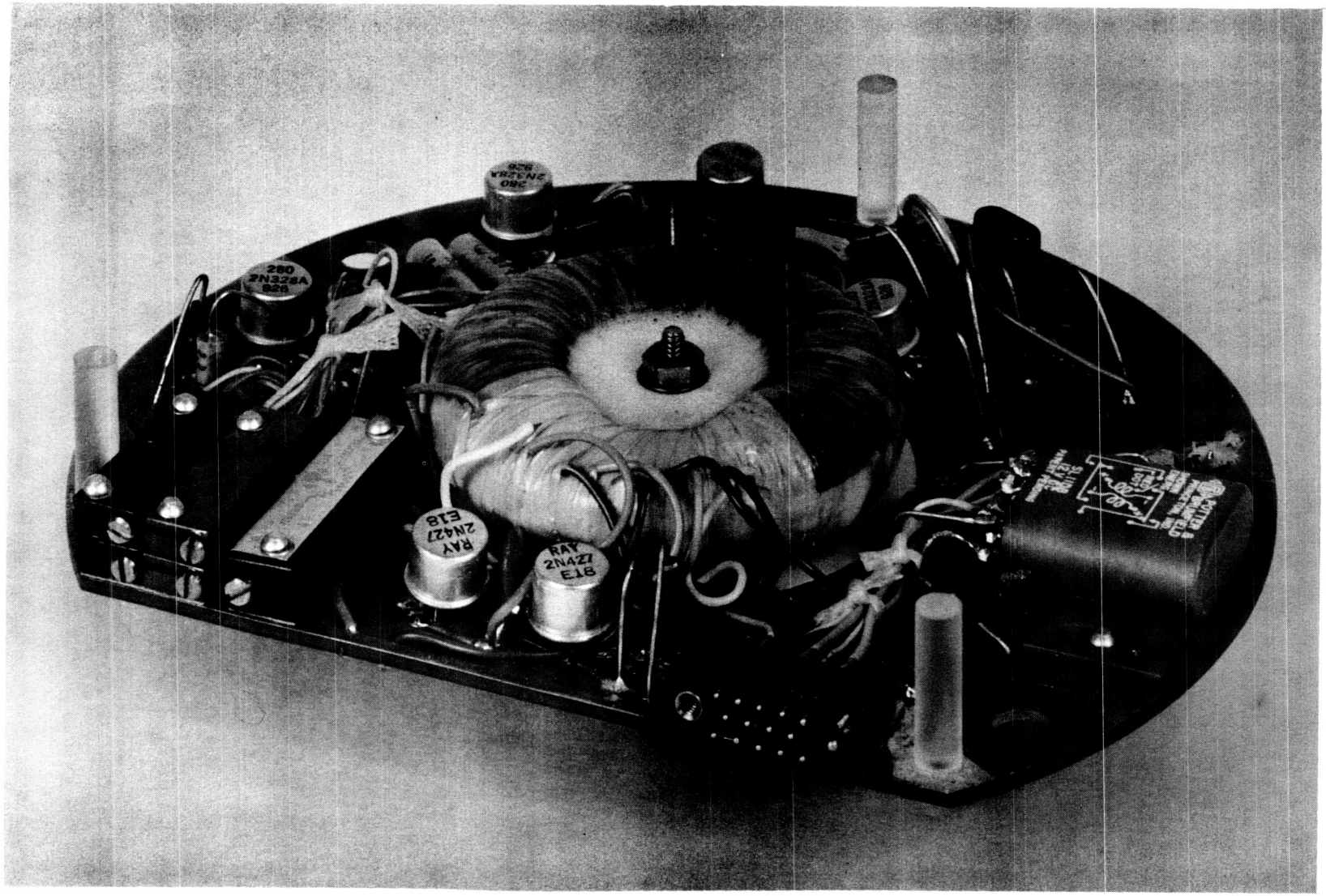

Figure 15 - Sweep generator

The second output is derived from the first by introducing a 180-degree phase shift and a fixed amount of attenuation. As illustrated in Figure 3, it is applied to the second and fourth grids of the multi-grid ion traps in order to minimize displacement currents.

8.8.7.2 Two electrometer amplifiers:

Two direct coupled amplifiers (Figure 16) are used to measure the six ion-trap and Langmuir-probe collector currents. Their use is time shared by use of a mechanical commutator inserted between the collectors and the amplifiers. Each amplifier has a dynamic range of 200 and is zero-centered to permit the measurement of both electron and positive ion currents. Feedback is used to insure long term stability. The minimum detectable current is 3×10^{-10} ampere. Range switching designed to achieve an overall dynamic range of 3×10^{-10} to 10^{-5} ampere is realized by use of a mechanical commutator.

8.8.7.3 Commutator:

The mechanical commutator consists of three solenoid-operated switching units. Two of the units provide for time-sharing of the two electrometer amplifiers by the six ion-trap and Langmuir-probe collectors. They also provide for current range switching for these collectors by successive application of collector load resistors. The third switching unit provides for time sharing of the main output of the sweep generator output with the two electric field meter outputs. There are nine distinct 10-second positions with an overall repetitive wave period of 90 seconds. The commutator provides three outputs to the telemetry encoder, the detailed time-sharing of which is illustrated in Table 2.

8.8.7.4 Electric-field-meter amplifier:

A simplified functional diagram of this module is presented as Figure 6. The two outputs, one proportional to the net diffusion current the other to the sheath field are time-shared with the main sweep generator output by use of the mechanical commutator inserted prior to telemetry encoder as detailed in Table 2. Both the field meter outputs are expected to vary with a period equivalent to the satellite spin period.

8.8.7.5 RF impedance:

The function of this module is to provide a basis for computation of the capacitance of the sensor, a shortened-dipole antenna. Figure 17 is a functional diagram of the module. The heart of the system is an oscillator whose frequency is determined in part by a sweeper and in part by the capacitance of the sensor. The start of the sweep is triggered by

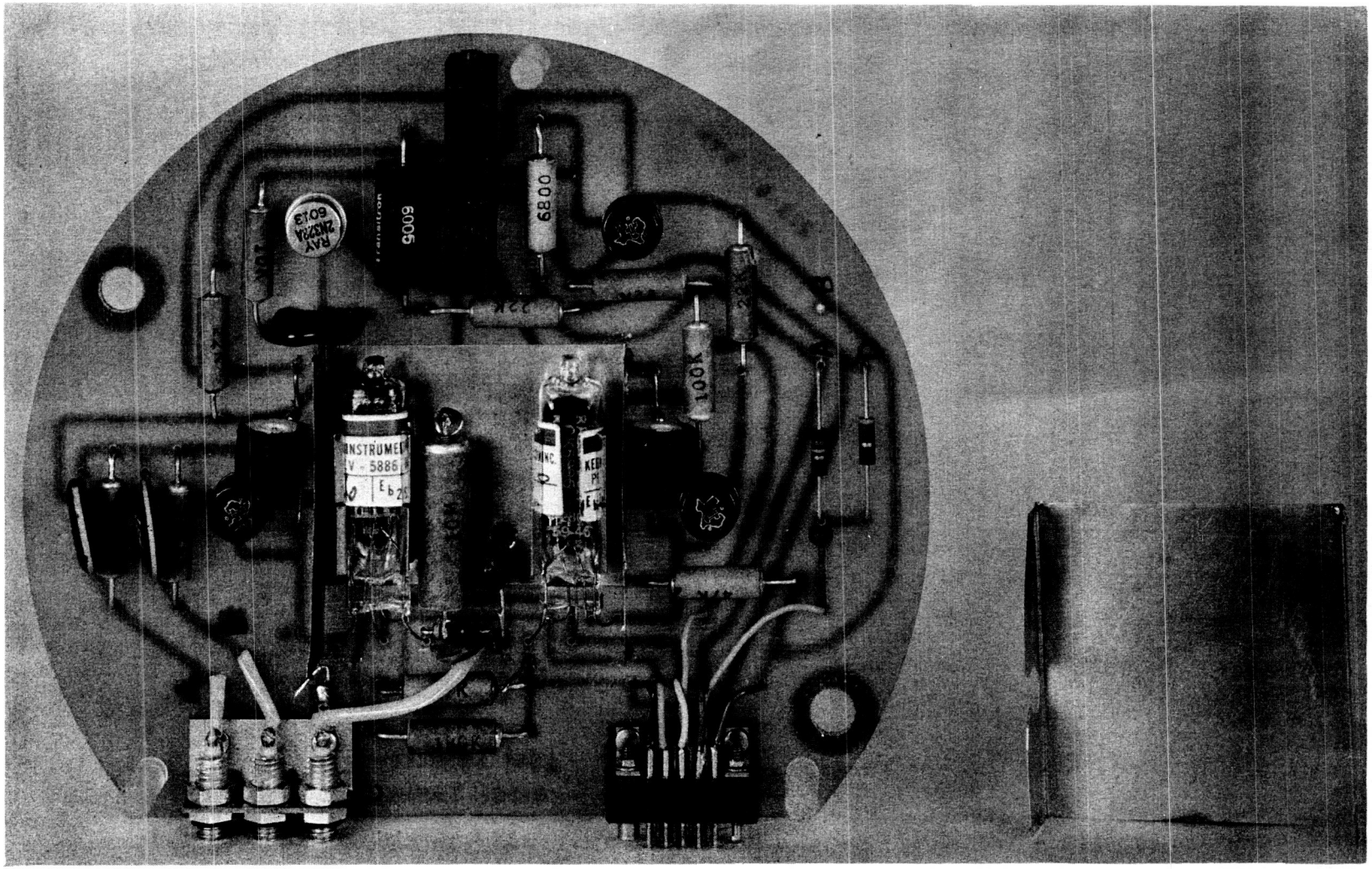

Figure 16 - Electrometer

Table 2

Mechanical Commutator Program

Time (sec)	Electrometer A Output	Electrometer B Output	Sweep-Voltage Field Meter
0-10	Langmuir Probe A Low Sensitivity	Langmuir Probe B Low Sensitivity	Sweep Voltage
10-20	Langmuir Probe A Medium Sensitivity	Langmuir Probe B Medium Sensitivity	Field Meter Current Density
20-30	Langmuir Probe A High Sensitivity	Langmuir Probe B High Sensitivity	
30-40	Single-Grid Ion Trap A Low Sensitivity	Single-Grid Ion Trap B Low Sensitivity	Field Meter Sheath Field
40-50	Single-Grid Ion Trap A Medium Sensitivity	Single-Grid Ion Trap B Medium Sensitivity	
50-60	Single-Grid Ion Trap A High Sensitivity	Single-Grid Ion Trap B High Sensitivity	Sweep Voltage
60-70	Multiple-Grid Ion Trap A Low Sensitivity	Multiple-Grid Ion Trap B Low Sensitivity	
70-80	Multiple-Grid Ion Trap A Medium Sensitivity	Multiple-Grid Ion Trap B Medium Sensitivity	Field Meter Sheath Field
80-90	Multiple-Grid Ion Trap A High Sensitivity	Multiple-Grid Ion Trap B High Sensitivity	

an 80-millisecond square wave developed by the rf memory computer from the 40-millisecond gate associated with the telemetry encoder. A crystal filter delivers an output pulse to the rf memory computer each time the oscillator is tuned to 6.5 Mc. Two of these pulses occur for each 80-millisecond period. The rf memory computer measures the time from the start of the sweeper output to the two output pulses. These time intervals which are a measure of the probe capacitance for two separate ranges of capacitances are delivered to the telemetry encoder by the rf memory computer in digital form.

As discussed in the description of the experiment, a bias obtained from the main output of the sweep generator is applied to the sensors on command to calibrate for the effects of an ion sheath which is expected to form around the probes.

Also contained on this module is a reference or calibration oscillator and crystal filter system. This functions identically to the probe

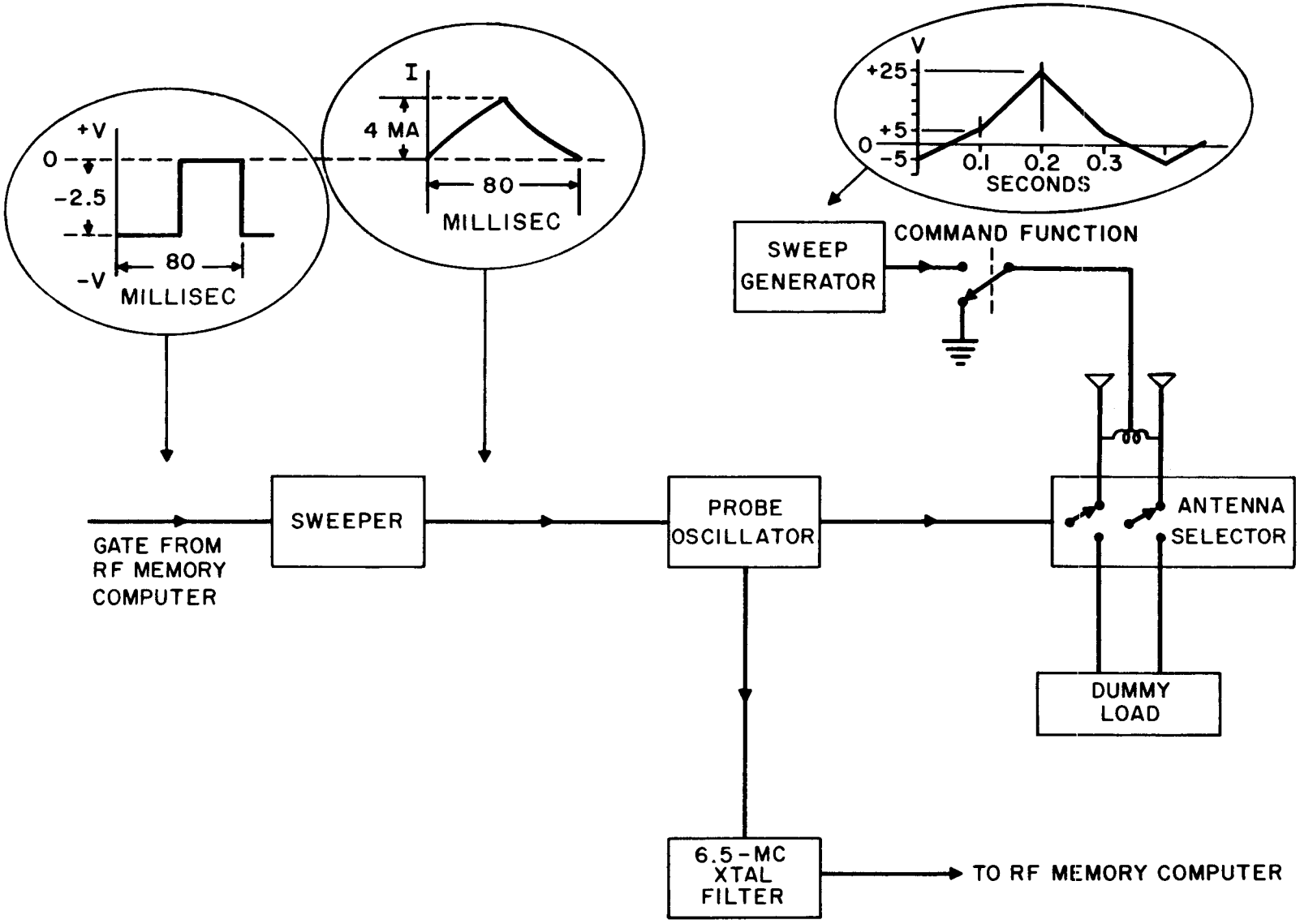

Figure 17 - Block diagram of rf impedance experiment

oscillator and crystal filter system except that dummy loads are applied in place of the sensor inputs. This reference system serves to calibrate for second-order drifts in the main oscillator system. The vacuum-temperature behavior of the dummy sensor will be known. Its capacitance will also be placed in digital form at the telemetry encoder input by use of the rf memory computer.

8.8.7.6 Command receiver and command program:

The quadriloop telemetry antennae are also used as the command receiver antenna. The command receiver is a single-channel system. When the receiver is actuated, the command program module (Figure 18) causes three events to occur simultaneously for a two-minute interval. The first event is application of power to the electric field meter sensor and amplifier. The second event is application of the variable bias to the rf impedance probe as described above. The third event is a calibration of the micrometeorite microphone experiment.

8.8.7.7 Aspect digitalizer, computer pulser and aspect memory:

These three units together combine the outputs of the solar and stellar sensors, and apply the information in digital form to the telemetry encoder.

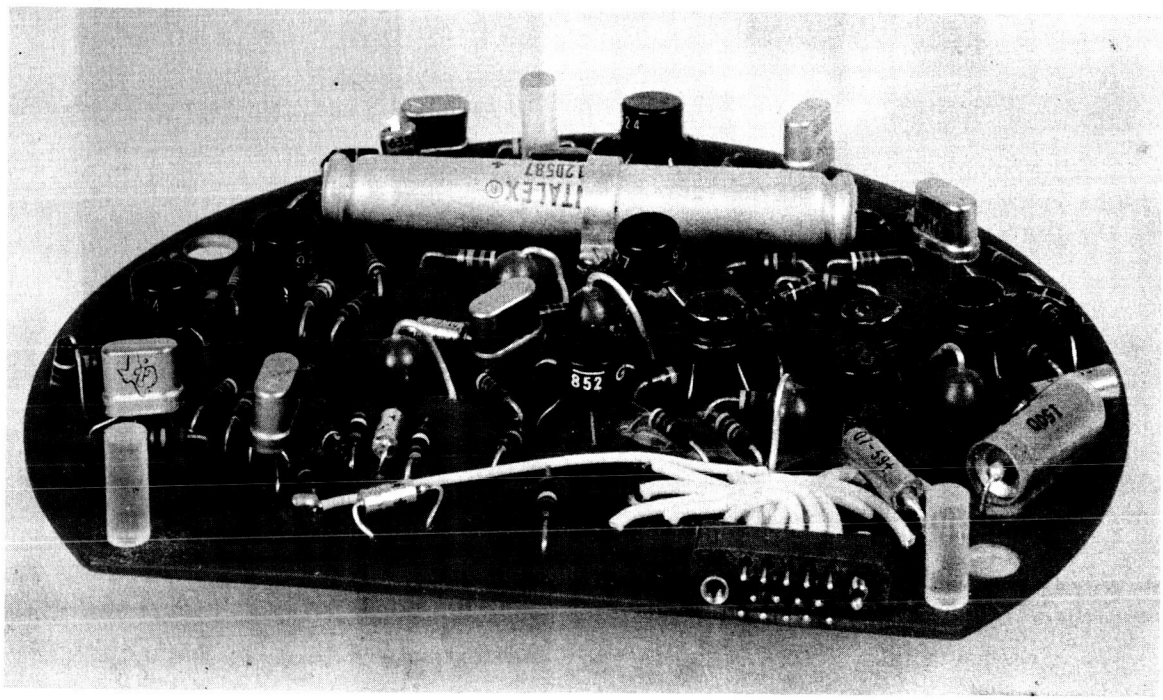

Figure 18 - Command program module

8.8.7.8 Meteorite amplifier:

The outputs from the two micrometeorite microphones are summed up at the input of a high-gain transistorized amplifier (Figure 19). Logic circuitry associated with the amplifier separates the information into three independent sensitivity ranges corresponding to three decades of particle momentum.

8.8.7.9 Meteorite counter:

The three outputs from the meteorite amplifier are stored separately by a very low current digital storage system. Information is read out at each satellite transit over a telemetry station. The storage system is designed such that for the expected frequency of impact it will not saturate over a period of time long compared to the time of one orbit. After saturation, the storage system recycles. The data is presented on the telemetry system in digital form.

8.8.7.10 Telemetry system:

The basic components of the telemetry system are two subcarrier oscillator modules, two encoder modules, and a transmitter. This system is described below. The weight distribution for Satellite S-30 is illustrated in Table 3.

8.9 Trajectory

8.9.1 Satellite Life

The minimum desired passive lifetime of the satellite is 6 months. The maximum expected active life of any experiment is approximately 3 months.

8.9.2 Perigee

A perigee as low as possible is desirable in order to compare the results of the ionosphere experiments with those from the existing worldwide network of ionosphere virtual height stations. Data from the virtual height stations are valid only up to F2 maximum, the altitude of which varies from 200 to 300 miles. The ideal perigee would be 200 ± 25 miles. The MSFC has recommended that to insure an orbit, the target perigee should be 275 miles with any dispersion error resulting in a lower value. A decision on the exact target perigee has not yet been reached.

8.9.3 Apogee

As was discussed under the objectives of the satellite, an apogee high enough that the altitude of the base of the exosphere can be determined from the

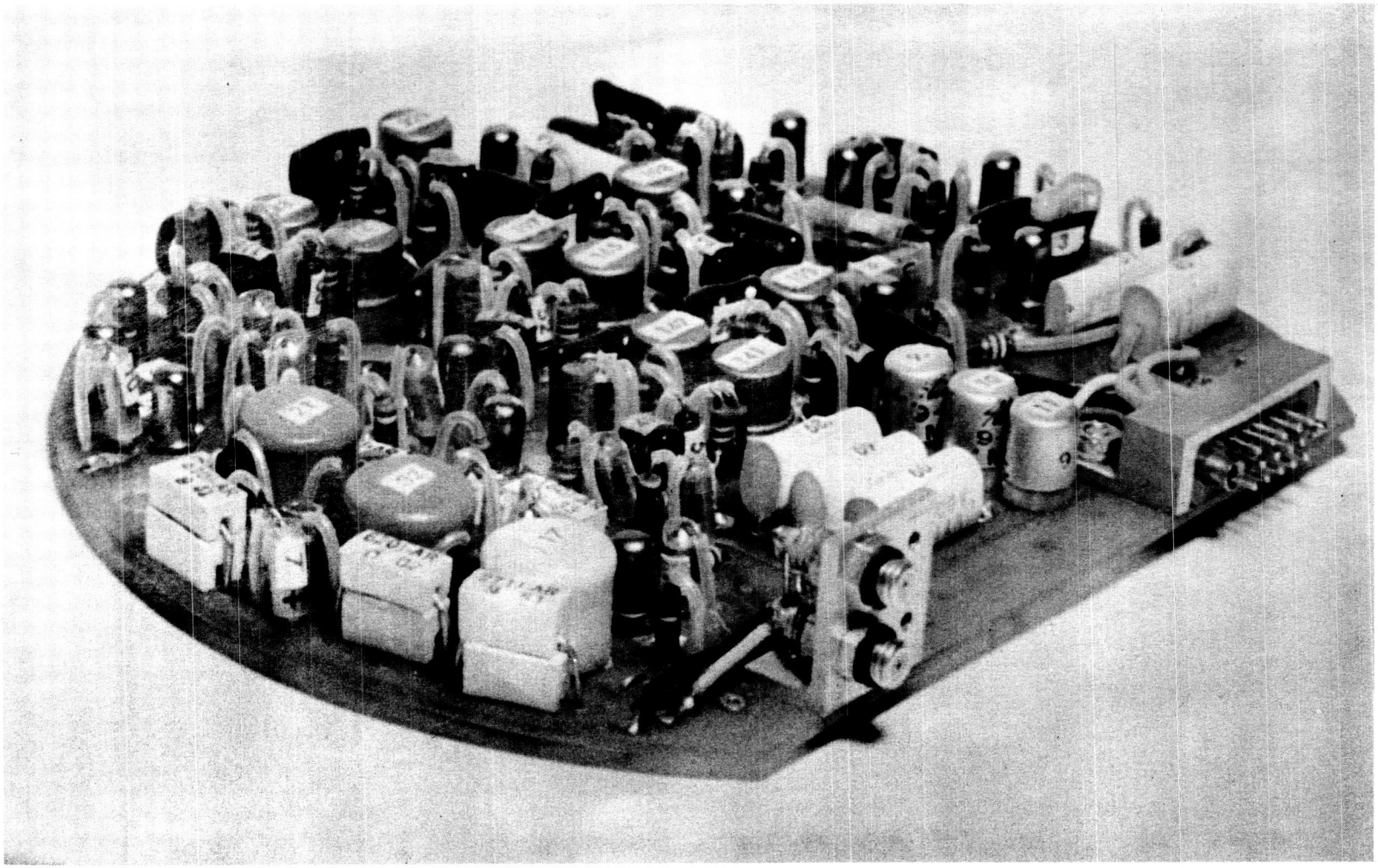

Figure 19 - Micrometeorite impactor amplifier and logic (S-30)

Table 3

Weight Distribution for Satellite S-30

ITEM		WEIGHT (lbs)
Structure		20.52
Main Batteries (including housings)		32.30
Instrument Column		11.90
Sensors		7.47
Multi-Grid Traps (2)	0.63	
Single-Grid Traps (2)	0.63	
Langmuir Probe (2)	0.63	
Electric Field Meter	0.75	
Meteorite Photomultiplier	2.20	
Aspect Sensor	0.50	
Sounding Boards	0.33	
Adapters	1.80	
First-Stage Despin		0.75
RF Impedance Probe		6.54
108-Mc Antenna Assembly		3.20
Battery for Separation Timer		1.20
Balancing Weights		0.70
Miscellaneous (Wiring, connectors, thermal coatings, special finishes)		6.42
Totals		91.1

ion mass distribution (ion trap data) is desirable. From this standpoint, a minimum apogee of 800 miles consistent with the perigee criterion has been requested. On the basis of a 92.5-pound payload weight, preliminary calculations show that a 1600-mile apogee is obtainable. This is considered too high in view of the desire to balance the amount of high-altitude and low-altitude data. It is expected that by launch time, a decision will be reached to use velocity cutoff to effect an apogee altitude of 900 ± 100 miles.

8.9.4 Inclination

The maximum possible inclination (51 degrees) for a Cape Canaveral launch is desired. The high inclination will permit the largest latitude coverage

for the measured ionosphere parameters, one of the primary objectives of the satellite. High inclination also will permit examination of micrometeor flux with respect to latitude. A significant micrometeorite measurement has not been obtained by the United States at latitudes greater than 30 degrees.

A high inclination is justifiable also from the standpoint of telemetry data acquisition. Since the Minitrack network will be used and the stations to be used are as far north as 40 degrees and as far south as 33 degrees, and because signal-to-noise ratios are marginal at apogee, anything lower than a 51-degree inclination would risk data recovery from almost half of the stations scheduled for telemetry acquisition.

8.9.5 Launch Time

The time of launch of Satellite S-30 will be determined once a firm firing date is established. The decision will be based on optimization of the following two factors: (1) In order to maintain as constant a package temperature as possible, the time will be chosen to minimize the possibility of the satellite being exposed to sunlight more than 65 percent of the time of a given orbit during the active satellite life. (2) Since some of the sensors located on the satellite equator are sensitive to photoemission, it is desirable that their exposure to direct sunlight on the light side of the orbit be spin modulated. Consequently, the angle between the spin axis and the sun's vector will be centered around 90 degrees during the 90-day active life of the satellite.

8.10 Stabilization

As discussed above the satellite spin rate will be reduced from 450 rpm to an initial orbital design value of 30 rpm. Some decay from the initial orbital value during the 90-day active satellite life is expected on the basis of magnetic drag. Simulated tests indicate that a value of less than 10 rpm can be expected after 90 days.

The satellite is being designed to maintain stability about the spin axis. A high moment of inertia is obtained by locating batteries on the periphery of the satellite's equator and by the weights placed at the ends of the two 10-foot rf impedance probes. Contributing to instability will be the fourth-stage rocket which will be carried with the payload for period of time after injection. A compromise will be made between stability and the risk of "bumping" by premature separation.

The following measurements of moment of inertia made on a prototype should be representative of the flight payload:

About the spin axis	27.74 in-lb-sec^2
Through c.g., perpendicular to thrust, direction, 10°	20.77 in-lb-sec^2

Through c.g., perpendicular to thrust, direction, 70°	21.71 in-lb-sec^2
Through c.g., perpendicular to thrust, direction, 130°	22.01 in-lb-sec^2

8.11 Power

Mercury cells (Figure 20) are used exclusively for the power sources of the S-30 experimentation. The batteries are of three types: RM-1, RM-12, and RM-42. To economize on weight, the experiments operate directly from the batteries so that no dc to dc conversion is used. A list of the batteries and their weights as applied to individual components, with data on the expected life of the component, is given in Table 4.

All components are operated continuously excepting the electric field meter which is active for 2 minute periods only on command. The total power consumption for this experiment is approximately 500 milliwatts. A total battery weight of 2.4 pounds is used. For this capacity and the expected frequency of command exercise, the experiment will be active for at least 2 months.

Table 4
Battery Weights and Expected Lifetimes for the S-30 Components

COMPONENT	VOLTAGE (volts)	POWER (milliwatts)	WEIGHT (pounds)	LIFE (months)
Transmitter	-18.2	278	11.0	2.00
Command Receiver	+11.7	33	0.8	1.65
Telemetry	+1.3 -2.6 -3.9	16	0.9	3.78
RF Impedance	-2.6 -13.0	163	3.6	1.40
Meteorite Microphone	±3.9 -7.8	43	1.0	1.3
Meteorite Photomultiplier	±3.9 ±7.8	64	2.0	2.3
Commutator	10.4	--	0.2	2.0
Sweep Generator	+26.0 +5.2 +2.6 -15.6	50	1.8	1.6
Electrometer	+1.3 ±10.4	40	2.2	1.8
Electrometer	+1.3 ±10.4	40	2.2	1.8
Aspect	----	--	1.2	1.0

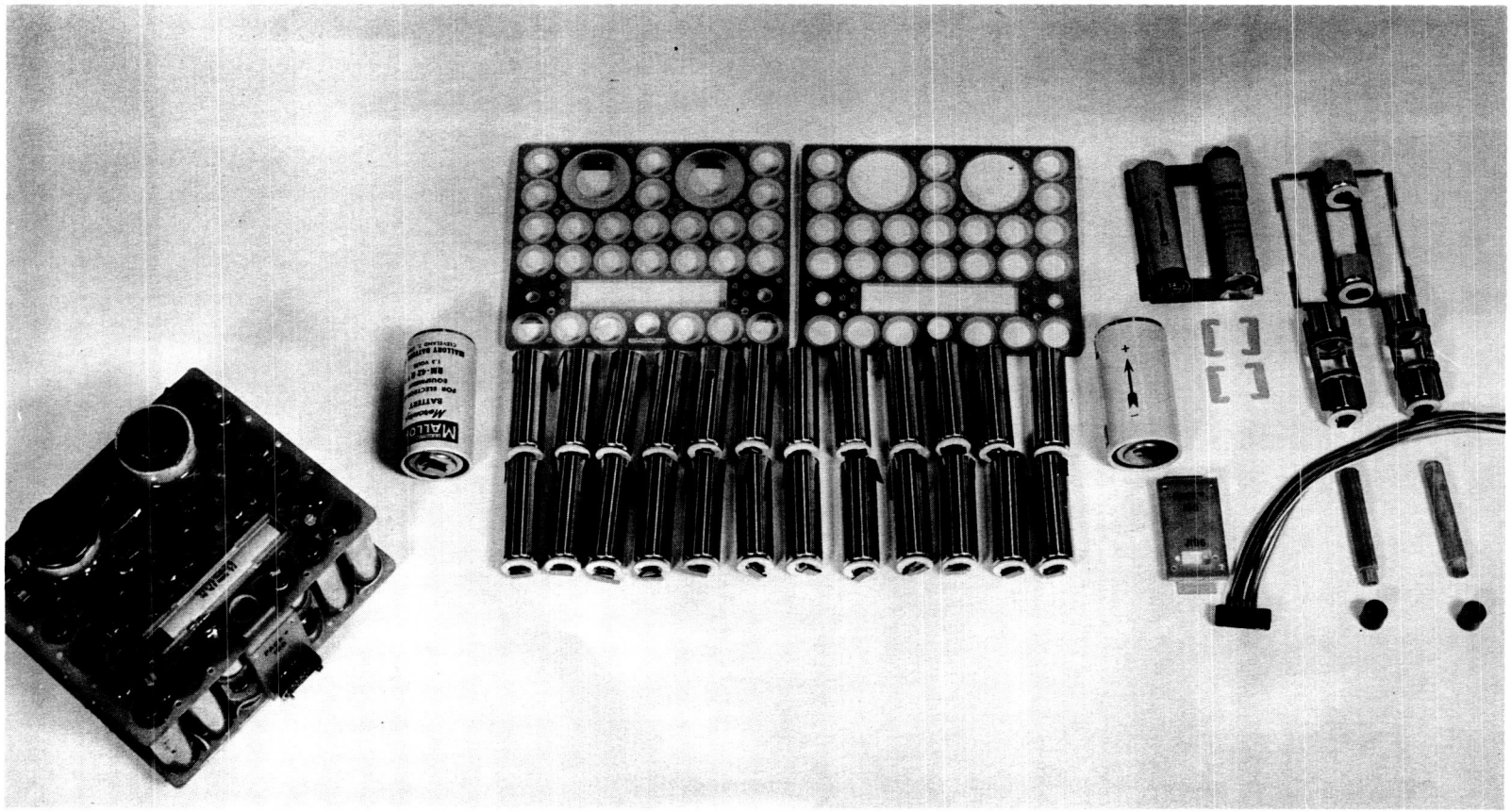

Figure 20 - Components of S-30 battery pack

8.12 Telemetry

The telemetry system on Satellite S-30 will operate continuously so that all data transmission will be real time. The system is a descendent of that used in the Vanguard system, meaning that the transmitter contains bursts of amplitude modulation separated by periods of no oscillation referred to as blanks. The long-term average radiated power output during modulation is 100 milliwatts. The 108-Mc antenna is the linearly-polarized quadriloop antenna (Figure 1) similar to that used on Explorer VII. The same antenna is used for the command receiver. For data acquisition, the required pre-detection receiver bandwidth is 60 kc. For this value, a predetection signal-to-noise ratio of 14 db has been computed at a 1000-mile range.

The basic element of time in the telemetry system is called a frame. Subcommutation is used so that analysis of two adjacent frames (termed A and B frames) is required to describe the complete picture. Tables 5 and 6 list the telemetry channel allocations for the A and B frames respectively. Blank 1 precedes Burst 1 in time, etc.

Two types of encoding are used: the frequency of modulation within a tone burst and the time duration of a blank between bursts. The only information coded in terms of the time duration of a blank are the temperatures measured at four different locations on the satellite. This encoding is the same for both frame A and frame B. For a temperature excursion of -10°C to +60°C, the time duration of these four blanks will vary from 0.5 to 1.1 milliseconds. Consequently, depending on the temperature at various points on the satellite, the time duration of the frames can vary from approximately 35 to 38 milliseconds. On either frame, A or B, the time duration of the 16th burst is made longer than the remaining 15 frames. This is done deliberately to provide a method of synchronization which serves to identify the start of a frame.

The frequency of modulation within the bursts are maintained within the range of 9 to 22.5 kc. The frequency modulation is presented either in digital form (8 discreet frequencies) or in analog form. Where the information is digital the period for 10 cycles of modulation is evenly distributed over the subcarrier range.

8.13 Tracking and Data Acquisition

Since the telemetry transmitter operates continuously, a separate tracking transmitter is not included. The minitrack network which successfully tracked from a similar telemetry signal during the Vanguard program will provide the major portion of the tracking information. The feasibility of using microlock for additional tracking information was established during prototype testing.

Steerable antennas with a gain of at least 20 db are required for the receivers to obtain telemetered data with adequate signal-to-noise ratios at apogee altitudes. For this reason, some of the "rocking-horse" antennas used in the Vanguard

Table 5

Telemetry Allocations (A Frame)

BLANK	TYPE	LENGTH	INFORMATION	BURST	TYPE	LENGTH	INFORMATION
1	--	1.4	--	1	D	1.2	Aspect Magnitude
2	--	1.4	--	2	D	1.2	Aspect Time
3	A	0.5-1.1	Instr. Col. Temp.	3	D	1.2	Met. Mic. Hi. Sens.
4	A	0.5-1.1	P.M. Temp.	4	D	1.2	Met. Mic. Hi. Sens.
5	--	1.2	--	5	A	1.2	Electrometer A
6	--	1.2	--	6	A	1.2	Electrometer B
7	--	1.2	--	7	A	1.2	S.V. - EFM
8	A	0.5-1.1	Skin Temp.	8	A	1.2	Met. Photom.
9	--	1.2	--	9	A	1.2	Electrometer A
10	--	1.2	--	10	A	1.2	Electrometer B
11	--	1.2	--	11	A	1.2	S.V. - EFM
12	--	0.4	--	12	D	1.2	RF Impedance
13	--	1.2	--	13	A	1.2	Electrometer A
14	--	1.2	--	14	A	1.2	Electrometer B
15	--	1.2	--	15	A	1.2	S.V. - EFM
16	A	0.5-1.1	Battery Temp.	16	A	1.45	Met. Photom.

program are being replaced by antennas with performance equivalent to the 108-Mc 22-db-gain 16-element yagi antenna now part of the Blossom Point installation. The expected data acquisition coverage from the Minitrack network, including the expected status of the receiving antennas, is given in Table 7.

In addition to the items listed in Table 7, the MSFC microlock station at Huntsville has been modified and will provide some data acquisition. The possibility of coverage from additional microlock stations is being investigated.

8.14 Data Processing and Reduction

Preliminary data processing and data reduction will be handled by the Tracking and Data Systems Divisions of the Goddard Space Flight Center. Details of the method of recording and of data processing are under preparation.

Table 6
Telemetry Allocations (B Frame)

BLANK	TYPE	LENGTH	INFORMATION	BURST	TYPE	LENGTH	INFORMATION
1	--	1.4	--	1	D	1.2	Aspect Magnitude
2	--	1.4	--	2	D	1.2	Aspect time
3	A	0.5-1.1	Instr. Col. Temp.	3	D	1.2	Met. Mic. Lo Sens.
4	A	0.5-1.1	P.M. Temp.	4	D	1.2	RF Impedance
5	--	1.2	--	5	A	1.2	Electrometer A
6	--	1.2	--	6	A	1.2	Electrometer B
7	--	1.2	--	7	A	1.2	S.V. - EFM
8	A	0.5-1.1	Skin Temp.	8	A	1.2	Met. Photom.
9	--	1.2	--	9	A	1.2	Electrometer A
10	--	1.2	--	10	A	1.2	Electrometer B
11	--	1.2	--	11	A	1.2	S.V. - EFM
12	--	0.4	--	12	D	1.2	RF Impedance
13	--	1.2	--	13	A	1.2	Electrometer A
14	--	1.2	--	14	A	1.2	Electrometer B
15	--	1.2	--	15	A	1.2	S.V. - EFM
16	A	0.5-1.1	Battery Temp.	16	A	1.45	Met. Photom.

Table 7
Expected Data Acquisition Coverage and Status of
Receiving Antennas at Minitrack Stations

STATION	LATITUDE	ANTENNA
Santiago	33°S	"rocking-horse"
Woomera	30°S	improved
Johannesburg	27°S	improved
Antofagasta	23°S	"rocking-horse"
Lima	12°S	improved
Quito	0°	improved
Antigua	23°N	"rocking-horse"
Ft. Myer	27°N	improved
San Diego	33°N	"rocking-horse"
Blossom Point	37°N	improved
North Dakota	47°N	improved

9. DIRECTIVES

None available at this time.

10. REQUIREMENTS YET TO BE SATISFIED

10.1 Determination of the precise orbital parameters and launch time have yet to be made and the predicted orbital parameters need to be provided to ground stations.

10.2 Final modifications of the Minitrack network (wide-band receivers and improved 108-Mc antennas) have yet to be completed. Operational plans for these stations need to be prepared.

10.3 Arrangements for the obtainment of virtual height station data to compare with the satellite perigee data need to be made.

10.4 Although compatibility of the S-30 telemetry system with microlock for tracking purposes was established, this needs to be checked with other microlock stations to insure monitoring of the injection sequence.

11. SCHEDULE

Prototype testing was completed on 9 July 1960. Three components which showed weaknesses will be tested again in modified form during 1 through 22 August. Fabrication of the flight models is expected to be completed by 29 August 1960. Flight acceptance tests are scheduled for the period 29 August to 9 October 1960. The satellite is scheduled to be launched during the last quarter of 1960.

12. FUNDING

The total funding including research and development, salaries and expenses for S-30 is listed below. The total does not include data acquisition, handling, and reduction since these items are not broken down by projects. The totals also do not include cost of the boosters.

12.1 In NASA

	FY 60	FY 61
12.1.1 Marshall Space Flight Center		
Design, fabrication testing of satellite shell.		
Design, fabrication and testing of despin devices.		
Design, fabrication and testing of rf impedance probe.		
Design, fabrication and testing of power supply.		
Design, fabrication and testing of rf matching networks.		
Design, fabrication and testing of separation components.		
Provide and operate facilities for prototype and flight acceptance tests.		
Mating of payload to Juno II upper stages.		
Field Services	585K	135K
12.1.2 Goddard Space Flight Center		
Payload Management		
Design of scientific experiments		
Calibration of scientific experiments		
Design fabrication and testing of all instrumentation except those listed above.		
Evaluation of prototype and flight acceptance tests.		

	Interpretation and reporting of data		
	Field Services		
		331K	197K
12.2	Contracts		
	Elgin Micronics for development and fabrication of commutators.	35K	6K
	Keithley Corporation for development and fabrication of electrometers.	12K	--
	Aero-Geo-Astrophysics Corporation for command receiver fabrication, rf impedance and sweep generator instrumentation fabrication and field services.	18K	10K
	Labko Scientific, Incorporated for development and fabrication of micrometeorite components.	75K	--
		140K	16K
12.3	Totals	1,056K	348K